Solution Based Growth of One-Dimensional ZnO Nanostructures and its Device Fabrication

By

Muhammad Awais Munawar

Reg. No.: NUST201260682MSCME67712F

Supervisor

Dr. Muhammad Israr Qadir

School of Chemical and Materials Engineering (SCME)

National University of Sciences and Technology (NUST)

2015

Solution Based Growth of One-Dimensional ZnO Nanostructures and its Device Fabrication

Name	Reg. No
Muhammad Awais Munawar	**NUST201260682MSCME67712F**

This work is submitted as a MS thesis in partial fulfillment of the requirement for the degree of

(MS in Materials and Surface Engineering)

Supervisor Name: Dr. Muhammad Israr Qadir

School of Chemical and Materials Engineering (SCME)

National University of Sciences and Technology (NUST)

Islamabad, Pakistan

2015

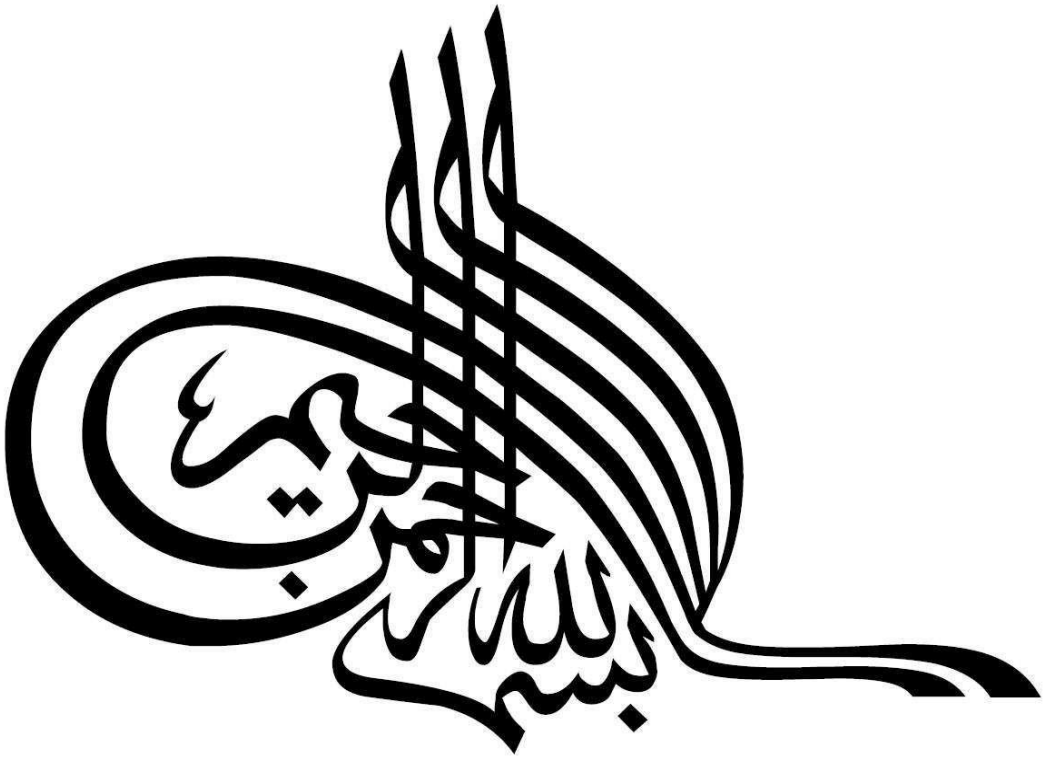

In the name of Allah,
the Most Beneficent,
the Most Merciful

DEDICATION

I would like to dedicate my work to

My beloved Parents

Haji Munawar Hussain, Farhat Perveen

Siblings

Mr. Muhammad Adeel Munawar

Mr. Muhammad Aqeel Munawar

Cute nephew

Abdul Hadee Ahmad bin Adeel

Teachers, Friends and everyone who ever pray for me..!!!

ACKNOWLEDGEMENTS

All the praises and thanks to **ALLAH Almighty**, the most merciful and compassionate, who is the entire source of knowledge and wisdom to mankind, who gave me ability and strength to complete this work successfully. I offer my humblest and sincerest Salam to **PROPHET MUHAMMAD (S. A. W.).**

Then I would like to thank my supervisor Dr. Mohammad Israr Qadir for his guidance and unconditional support throughout the course of this work. Sir, I am very grateful for the time you have dedicated to me, your suggestions and useful discussions. Thank you also for the friendly environment in which you have welcomed me. All this has been of great support, helping me to face the ups and downs of my project, which I do not think I would have completed it otherwise. I am extremely thankful to my parents and family whose prayers have been a driving force for me. Especially to the support of my elder brother Mr. Muhammad Adeel Munawar. My profound regards for each teacher who has directly or indirectly taught me in life. May Allah reward them with His blessings for their efforts.

Next, I would like to thank my friends who have supported me throughout the years. Special thanks to my friend Mr. Zeeshan Ali, who supported and helped me in throughout of my MS degree. Mr. Aftab Akram, who helped me in different characterization tools. Regards to all lab engineers, technicians and other staff members for making life easier at SCME. Special thanks to Mr Shamsuddin (SEM Lab) for assisting and teaching me about the electron microscopy. Regards to Mr Khurrum (XRD Lab), Mr Imran (Nano-Synthesis Lab), Mr. Zafar Iqbal (surface lab) and Saqlain Bhai who have been supportive in different phases of the work at SCME.

ABSTRACT

The whole world is replacing high energy consumption conventional light sources with low energy consumption light emitting diodes because LEDs are more economical and easy to fabricate, low energy consumption, hazardless and highly friendly to the environment. ZnO is one of the most promising wide band gap semiconductor compounds due to a unique combination of properties which renders it ideal for optoelectronic applications especially for the LEDs.

A low temperature solution based technique was utilized for the fabrication of one-dimensional (1D) nanostructures of n-ZnO semiconductor material on a substrate containing thin film of p-doped semiconductor material. Scanning electron microscope, X-rays powder diffraction, Fourier transforms and UV-Vis spectroscopies as well as photoluminescence measurements were performed to investigate the diverse characteristics of synthesized 1D nanostructure which further processed for the fabrication of light emitting nanodevices (LEDs). Finally, the fabricated nanodevice was further investigated through the electroluminescence measurements to look the emission spectra and the quality of the light. The combination of the design of LED based on merely solid state materials and nanoscale materials grown at nearly room temperature holds the capabilities to produce the lighting devices at much lower cost compared to conventional LEDs available in the market and this design could pave the way to fabricate the new lighting solid state sources.

CONTENTS

LIST OF FIGURES

LIST OF TABLES

LIST OF ABBREVATIONS

LEDs	Light Emitting Diodes
HMT	Hexamethylenetetramine
HF	Hydrofluoric Acid
CBD	Chemical Bath Deposition
RPM	Round per Minute
NPs	Nanoparticles
NRs	Nanorods
NM	Nanometer
AFM	Atomic Force Microscopy
SEM	Scanning Electron Microscopy
FTIR	Fourier Transforms Infrared Spectroscopy
XRD	X-ray Diffraction
UV	Ultraviolet
PL	Photoluminescence
EL	Electroluminescence

1. Introduction

Light-emitting diodes (LEDs) have considerable potential for the source of general light applications. These have the potential of ten times more efficient than the conventional light sources. So the whole world is replacing the high energy consumption conventional light sources with low energy consumption LEDs. It will decrease around 20% of energy consumption. The U.S. Department of Energy (DOE) states that $120 billion can be saved for the period across 2010-2030 at today's energy prices by replacing conventional lighting with LEDs. It will also decrease 246 million metric tons of carbon emission in the environment.

Since the last decade, attention of worldwide research in semiconductor materials has been focused on zinc oxide (ZnO) because of its outstanding semiconductor properties. ZnO has great potential in an extensive range of uses like laser, transparent electronics, optoelectronics and sensing applications due to its suitability and controllable properties like high thermal conductivity, high mobility of electron, wide band gap (3.37 eV), high transparency, high exciton binding energy (60meV) and easy methods for the growth of its nanostructures [1-4]. After Si, ZnO has become the second most popular semiconductor material in 2007 and the number of publications on ZnO is still increasing with time [5].

It is a very difficult task to obtain reliable, controllable, high conductive and reproducible p-type doped ZnO [6, 7]. The formation of low energies due to intrinsic donor defects like oxygen vacancies (V_o), zinc interstitials (Zn_i), which can compensate acceptors are responsible for it. Excellent properties of ZnO can be utilized by fabricating heterojunction with other semiconductors. To control the emissions of LED by utilizing the optical properties of ZnO, p-n heterojunctions can be constructed by growing n-ZnO nanostructure on any other p-type semiconductor materials. With different p-type semiconductor materials such as Si, GaN, GaAs, CdTe and diamond, different heterojunctions of ZnO nanostructures have been obtained [8-10]. To fabricate LEDs with n-ZnO, p-GaN is an excellent material for the construction of heterojunction. Both semiconductor materials ZnO and GaN have

similar properties such as the lattice parameters, wurtzite crystal structure and band gap (3.37 eV and 3.4 eV respectively).

Different fabrication methods for different complex device structures have been reported. Different undoped or insulating layers were inserted in n-ZnO nanorods/p-GaN to modify their structure, but in comparison with simple n-ZnO/p-GaN based LEDs, these layers changed the emission spectrums [11-13]. The emission spectrum of n-ZnO nanostructure/p-GaN heterojunction based LEDs have covered the whole visible spectrum which makes it a strong candidate for white light source. The comprehensive studies of n-ZnO nanostructures/p-GaN based LEDs are still under research and have a large area of interest. ZnO nanostructures/p-GaN based LEDs have special interest due to its low cost fabrication methods. ZnO nanotubes and nanorods based LEDs have the ability to improve light extraction as reported in the literature [14]. Low cost aqueous chemical growth (ACG) method was used in this research work for synthesis of ZnO nanorods on p-type GaN substrate to fabricate the p-n heterojunction LEDs. Different properties were investigated of the developed LEDs like luminescence, crystal structure, surface morphology, chemical composition and color quality.

However, ZnO has strong potential to compete with the most leading commercial material GaN for the fabrication of LEDs. But the achievement of controlled origin of visible emissions is still a challenge after investigations for decades.

1.1 Main Objectives

The main objectives of this research are

- Growth of 1D ZnO nanostructures by Chemical Bath Deposition
- Investigate the effect of seed layer parameters on the final growth of ZnO nanorods.
- Investigate the effect of time and temperature on length and diameter of ZnO nanorods.
- Control of diameter and length of ZnO nanorods
- Characterization of material such as crystal structure, surface morphology, optical properties by using XRD, SEM, FTIR, UV-visible Spectroscopy.
- Device Fabrication

- Electrical and Luminescence properties of fabricated device.

This thesis describes the whole research in this way; chapter 2 covers the basic introduction of ZnO and its basic properties. A brief discussion about physical, luminescence and electrical properties of ZnO are also given. Some basic applications of ZnO nanostructures are also discussed like UV detectors LEDs and bio sensing. Chapter 3 covers the experimental method used to grow the one-dimensional ZnO nanostructures and Chapter 4 includes the characterization techniques used. Chapter 5 describes the results and discussion of this research work which summarizes the entire research effort and final Chapter 6 focuses on the conclusions with future recommendations.

2. Literature Review

2.1. Zinc Oxide (ZnO)

Recently, new nanostructures/nanomaterials based device have shown the great potential due to their attractive properties for sensors, optoelectronic devices and electronic applications. These make ZnO a favorable material due to its fascinating properties for the fabrication of nanodevices such as light emitting diodes (LEDs), sensing devices, nanogenerators and UV detectors [16-19]. So it is the most utilized semiconductor material right now between all the metal oxides due to its excellent semiconductor, piezoelectric and optical properties. Some of the basic properties of ZnO are described below:

2.1.1. Semiconductor ZnO Basic Properties

Normally, the formation of ZnO crystal structure is hexagonal (wurtzite) as shown in figure 2.1, with lattice parameters a = 3.25 Å and c = 5.12 Å. The strong ionic bonding between Zinc and oxygen is due to differences in their electronegative values (Zn = 1.65, O = 3.44). The tetrahedral coordination of Zn atoms with four oxygen (O) atoms which alternatively arranged along with c-axis makes the wurtzite structure. Generally, the neutral unit cell of ZnO consists of an oxygen anion covered by four zinc cations at the tetrahedron corners. Polar surface is formed due to negatively and positively charged surfaces. These surfaces occur when anions and cations entirely terminated some surfaces due to the crystallographic configurations. These are the non-convertible and fixed ionic charges polar surfaces. Different 1D structures are formed due to the presence of high surface energy like nanorods, nanowires, nanocages, nanosprings, nanobelts and nanotubes [20, 21].

Generally, wurtzite structure of ZnO consists of two polar surfaces. The polar surface has Zn (0001), O $(000\bar{1})$ faces ended along c-axis. The non-polar surface has the same amount of O and Zn atoms having planes $(10\bar{1}0)$ and $(11\bar{2}0)$ respectively. Different physical and chemical properties of ZnO are due to these polar surfaces.

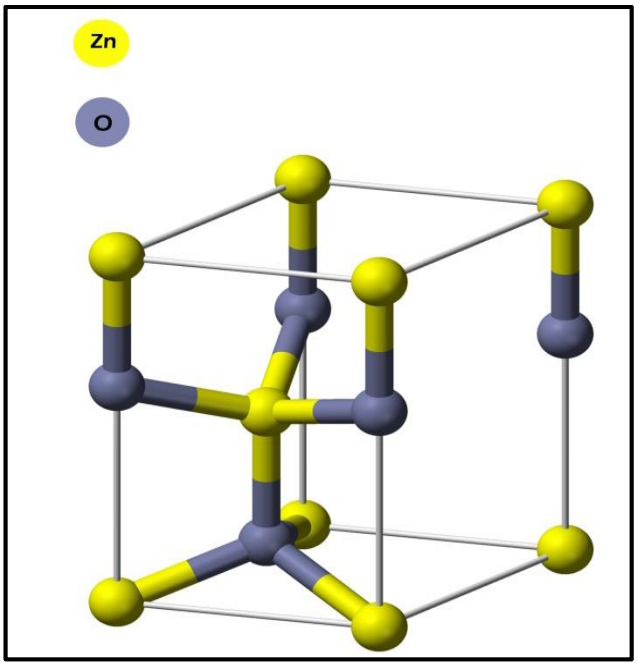

Figure 2.1: ZnO unit cell with Hexagonal wurtzite structure showing tetrahedrally co-ordinated zinc and oxygen ions**.**

The positively charged Zn at (0001) plane and negatively charged O at $(000\bar{1})$ plane are formed due to the polarized charged ions. Immense surface restorations occur by polar surfaces to obtain the stable structure, except for atomically flat, stable ± (0001) face of ZnO. The excellent stability of the ZnO polar surfaces ± (0001) makes it the most leading research areas in the field of surface physics. At pressure of 10GPa, the phase conversion occurs in ZnO wurtzite (B4) structure which transforms it to rock salt (B1) [22-25].

ZnO nanostructured materials have different properties depending upon different factors such as growth, polarity, etching, plasticity, piezoelectricity, impulsive polarization and generation of defects. ZnO has more advantages in comparison with other semiconductor materials like GaN because of its ambient high exciton binding energy and direct and wide bandgap. ZnO has the exciton binding energy of 60 MeV, but GaN has 25 MeV. The efficiency of light emission depends on this exciton binding energy. Several comprehensive analyses have been reported in literature on various characteristics of ZnO material [26].

2.1.2. Basic Physical Properties of ZnO

Some of the physical properties of ZnO are shown in Table 2.1 [27, 28]. Mobility carrier's values can be improved after getting control on the defects in the

structure. It's a challenging task to achieve a stable form of p-type doped ZnO. The effective mass and mobility of holes related values are still under moot [29].

Table 2.1: Basic room temperature physical properties of ZnO [27, 28].

S. No	Factors	Values
1	Bandgap energy	3.37 eV
2	Exciton binding energy	60 MeV
3	Lattice parameters	a = 0.32495 nm, c = 0.52069 nm
4	Molecular mass	81.389 g/mol
5	Density	5.67526 g/cm^3
6	Melting point	2250 K
7	Electron mobility	~210 cm^2/Vs
8	Effective mass of Electron	0.28 m0
9	Effective mass of Hole	0.59 m0
10	Refractive index	2.008, 2.029
11	Static dielectric constant	8.656
12	Thermal constant at 573	1200 mV/K
13	Specific heat	0.125 cal/g°C
14	Thermal conductivity	0.6 – 1.16 W/Km

2.1.3. Defects and Optical Emissions of ZnO

Extrinsic and intrinsic defects are responsible for the optical and electrical properties of semiconductors. These defects are present in the crystal structures. ZnO with its wide bandgap (~3.37 eV) has strong potential to be used in photonic applications in range of UV or blue spectra and its high exciton-binding energy (60 MeV) permits ZnO for the efficient excitonic emission. ZnO becomes very attractive in optoelectronics applications due to its efficient radiative recombinations. Various techniques are in use to measure both structures (bulk and nanostructures) of ZnO for its photosensitive/luminescence properties at low and room temperatures. Figure 2.2 shows the room temperature PL and EL measurements of two different ZnO nanostructures based heterojunction LEDs.

Broad visible emissions and ultra-violet (UV) emissions have been measured in photoluminescence spectra. The transition recombination of free excitons is responsible for ultra-violet peak in the near band-edge of ZnO. With

neutral and charged states, the excitons may be limited to only accepters and donors or they can move freely through the crystal [16]. As shown in the above figure 2.2, the presence of surface defects in structure is responsible for the broad visible region, ranging from 420 nm to 750 nm in ZnO. By varying these defects, the electrical and optical properties of ZnO can also be changed. There are many techniques that can be used to introduce these defects like during the fabrication process, by ion implantation or by post annealing.

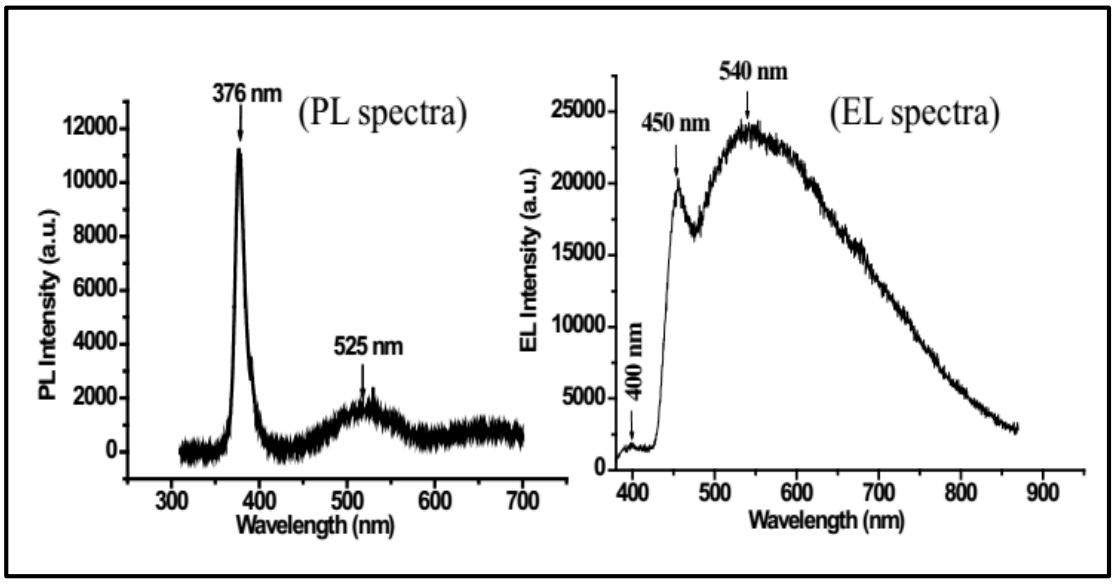

Figure 2.2: Room Temperature PL and EL measurements of ZnO nanoflowers and nanorods based LEDs respectively [16].

Extrinsic and intrinsic defects are responsible for the optical properties of ZnO and still arguable. Specially, the intrinsic emission's origin from ZnO is still under moot. The donor energy level exists below the conduction band (CB) and acceptor energy level present above the valence band (VB). The near-band edge emission is due to these donor and acceptor energy levels and the deep energy levels within the bandgap are responsible for the whole visible region emission (400-750 nm). The source of these defects is still under research and different origins for these deep level defects have been reported [30]. Three types of defects exist in the crystal structure, point, line and complex defects. Point defects occur due to inaccessible atoms in localized regions, whereas the dislocations into the rows of atoms generate line defects and the combination of point defects forms complex defects. The combinations of impurities are responsible for extrinsic point defects in the structure and host atoms generate intrinsic defects. Holes and electrons present in the valence band and the conduction band respectively cause the intrinsic optical recombination.

The whole visible range (400-750 nm) or deep level emission (DLE) band in ZnO depends on the several intrinsic defects in the structure.

These intrinsic defects could be the oxygen interstitial (O_i), oxygen vacancies (V_o), zinc interstitial (Zn_i), zinc vacancies (V_{Zn}), zinc anti-site and oxygen anti-site. Green emission from ZnO depends upon ionized oxygen vacancies. While for the red emission from ZnO, doubly ionized oxygen vacancies are responsible [31-33]. Several reports report on green emission of ZnO. It has been reported that source of green emission has origin under the conduction band at 2.4-2.6 eV in ZnO. It has also been reported that oxygen vacancies might also responsible for green emission in ZnO. Some researchers also reported that the V_o and V_{zn} both contribute to the green emission along with many deep level defects. In ZnO, the blue emission also considered to be the result of zinc vacancies. The recombination of zinc interstitial (Zn_i) energy level and V_{zn} energy level also make blue emission. The blue emission range is ~ 2.84 eV (436 nm). This phenomenon may be defined by full potential linear muffin-tin orbital method. This method describes the position of V_{zn} that positioned at ~ 3.06 eV below the conduction band, while Zn_i level position is hypothetically calculated at a position below the conduction band at ~ 0.22 eV [34]. These defects are intrinsic in nature. In ZnO generally zinc interstitial defects situated at ~ 0.22 eV under the conduction band. Recombination in different defects present in deep levels and Zn_i defines this phenomenon. The deep level defects such as oxygen interstitials, oxygen and zinc vacancies are responsible for different color emissions like red, green and blue emissions in ZnO [34]. Oxygen interstitials defects generate orange-red emissions in ZnO and normally positioned below the conduction band at 2.28 eV [35, 36]. As reported in literature, yellow emission is also due to the oxygen interstitials defects. Yellow emission can also be observed by adding O_i and Li impurities as reported by some research groups. During the chemical growth process, attachment of Zn $(OH)_2$ on the surface of the nanorods is also responsible for yellow emission. By occupying of wrong lattice position, ZnO structure also generates some anti-site defects. These defects are generated by the replacement of zinc position with oxygen or oxygen position with zinc. By applying the irradiation processing or ion implantation, these defects can be merged into ZnO. Some cluster defects are also generated by the agglomeration of point defects in ZnO. These defects can also be generated when oxygen vacancy and zinc interstitial

merged to form V_o Zn_i cluster and it's positioned below the conduction band at 2.16 eV.

Extrinsic defects are also a major cause of different emissions in ZnO. In ZnO, the UV emission is placed around 3.35 eV depends on the recombination of extrinsic defects to excitons. The emission positioned at 2.85 eV is due to merging of Cu impurities in ZnO. Also, a yellow emission was observed below the conduction band positioned at 2.2 eV in Li doped ZnO. The other extrinsic defects which make different emissions from ZnO are caused by the doping of Cu, Li, Fe, Mn, and Mg. The emission of same colors can also be observed from the defects of different energies such as ZnO: Co and ZnO: Cu emits the same emission (green) but these combinations have dissimilar energies. Finally, hydrogen related defects are also responsible for different emissions from ZnO. These are not deep level defects and positioned below the conduction band at 0.03 to 0.05 eV [35]. So it shows that ZnO emissions cover the whole visible region and it is the most favorable material for the use of low power consumption white light emitting sources.

2.1.4. Electrical Properties of ZnO

The fabrication of nanostructures into nanodevices can be described by the electrical performance of ZnO. The presence of naturally occurred ZnO crystal structure defects such as oxygen vacancies and zinc interstitials make it n-type semiconductor material as reported in the literature [36]. At room temperature, numerical values of the estimated electron mobility are 120 to 440 cm^2 V/s in an undoped ZnO nanostructure and still under moot. It also depends on the methods of fabrication, and measured values for highest carrier concentration in doped ZnO are 1019 cm^{-3} and 1020 cm^{-3} for holes and electrons respectively. However, these p-conductivity levels are uncontrollable and not reproducible. In comparison with undoped ZnO, the carrier mobility of doped ZnO has reduced as reported in literature. The mechanism of carrier scattering is responsible for this. This mechanism describes the different scatterings like ionized and non-ionized impurity, acoustic and polar optical-phonon scatterings. The estimated values were 200 cm^2 V/s and 5 to 50 cm^2 V/s for the mobility of electrons and holes respectively at ambient temperature, and estimated values of electron and hole effective mass were 0.24 m_0 and 0.59 m_0 respectively. Due to the large differences in effective mass, it has been shown that the electrons have very high mobility than holes [36].

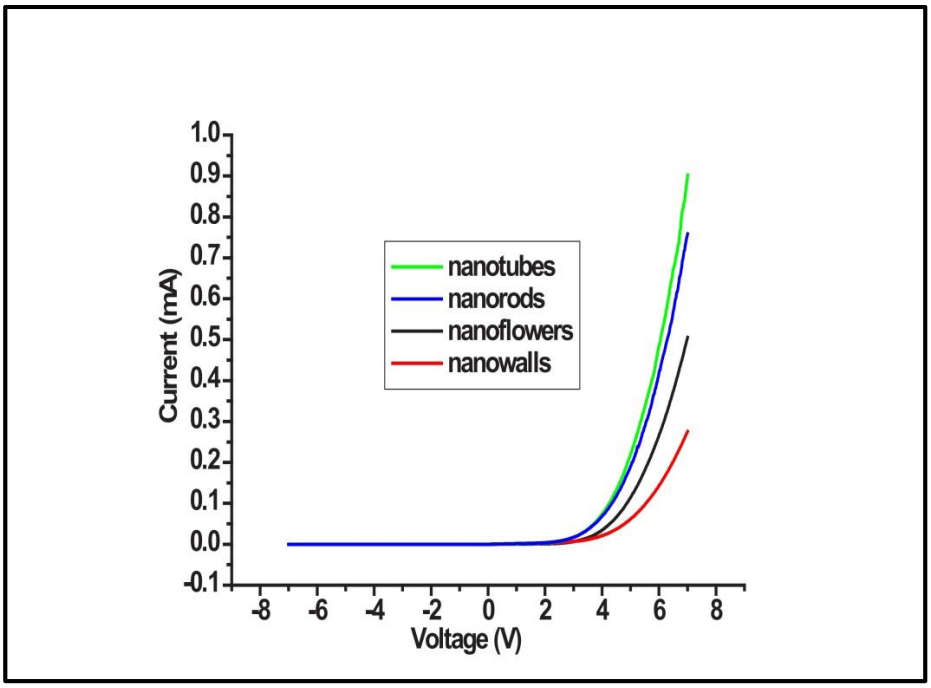

Figure 2.3: I-V curves of different ZnO (nanostructures)/p-GaN based LEDs [16].

The ZnO nanostructures based p-n heterojunction LEDs have been developed as reported [16]. Figure 2.3 shows the typical I-V curves i.e electrical parameters of these fabricated LEDs. A good rectifying behavior was estimated of the different LEDs. The stable p-n heterojunctions were attained and these LEDs showed around 4V of threshold voltages. In comparison with other nanostructures based LEDs, the ZnO nanotubes based LED shows advanced current with same operating states. It may be due to the large surface area of nanotubes and more oxygen sub-vacancies in its structure.

2.2. Applications of ZnO Nanostructures

ZnO is a very attractive semiconductor material for applications in photonics, electronics, sensing and acoustics. It has excellent chemical, optical, electrical, mechanical and piezoelectric properties. Due to several reasons such as excellent optical properties and low production cost, ZnO is being used as an alternative to GaN for device applications. ZnO becomes superior over other semiconductors because of its high exciton binding energy. The stable p-type ZnO attainment is still under moot among the research community and main hurdle in the fabrication and development of ZnO based p-n homojunction optical devices. ZnO has great potential to be used in biosensors, acoustic wave resonators, gas sensors and solar cell device applications. Due to high transparency, it is also very attractive

material for transparent electronics. ZnO has a wide range of nanostructures. These ZnO nanostructures are being used in a wide range of nanodevices like, LEDs, bio-sensors, UV detectors, gas sensors and nano-generators and bulk acoustic wave resonators (BAW) [36-39].

2.2.1. ZnO based UV Photodetectors

ZnO has become attractive material for ZnO based ultra-violet (UV) photon detection due to its excellent electrical, structural and optical properties. So it is an appropriate material for the production and development of UV detectors having a high performance detection. These detectors are chemically stable, low cost and environment friendly (radiation resistant). So these detectors can be used in civil, military, nuclear and space applications. In 1940, the first UV photo-response in ZnO thin films was detected. In the beginning, the fabricated ultraviolet detectors had not so good properties, but the research increased gradually on ZnO based photo detectors in 1980. Different methods have been implemented for ZnO thin film based UV detectors to increase their efficiency. Different ZnO based photo-detectors including Schottky photodiodes, metal-semiconductor-metal photo detectors and photoconductors have been reported in literature [41-43]. Recently single nanowires-based UV photo-detectors have been fabricated for fast switching. Schottky photodiodes have many advantages such as high response speed, high UV/visible contrast, low dark current and have zero bias operating possibility. These advantages make it superior over metal-semiconductor-metal photodiodes and photoconductors [30]. In 1986, first ZnO based Schottky diode was fabricated [43]. Different methods for ZnO based Schottky photodiodes have been reported by different research groups [36].

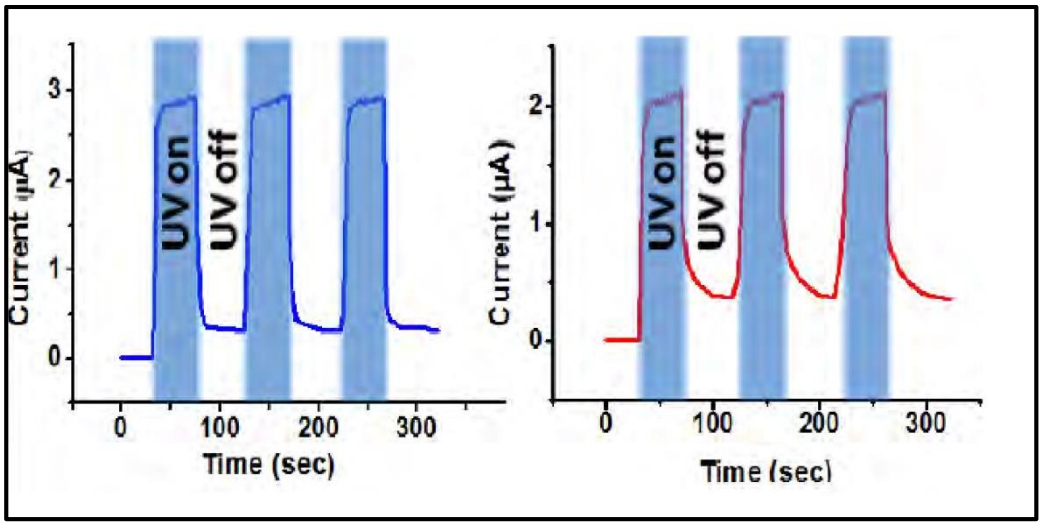

Figure 2.4: Single ZnO nanowire hoto-response by a 365 nm wavelength UV light with (a) Schottky contact on one side, and (b) ohmic contacts on both sides [44].

Schottky diodes were fabricated by a using single long (30 μm) ZnO nanowires. These diodes were also compared with diode having ohmic contacts. These Schottky diodes showed rectifying behavior with no reverse breakdown up to -5 V and high current under forward bias. These fabricated Schottky diodes also showed stability up to 12 V as shown in figure 2.4, these fabricated Schottky diodes showed high sensitivity and faster switching [44].

2.2.2. Light Emitting Diodes (LEDs)

The artificial lighting has become the essential part of our modern human society. USA used 20% of its total generated electricity for the general lighting purpose. Development of the efficient and environmentally friendly white light sources has become the endless desire of the society. Light emitting diodes (LEDs) based light sources can decrease 50% electricity consumption for light sources. These can also decrease the environmental pollution threats as well. The major cause of environmental pollution is conventional light sources, it adds 1900 million tons of CO_2 each year in the environment. So conventional light sources are less reliable than LEDs based light sources. The incandescent and fluorescent lamps have 1000 h and 10000 h of lifetime respectively. The output power of fluorescent lamps decreases and absorption within the lamp increases because these lamps use phosphors for white light generation. To overcome this problem, the researchers build their interest to develop hybrid LEDs. They utilized the excellent optical properties of ZnO by fabricating ZnO heterojunctions with other p-type

semiconductor materials like Si, GaN, SiC, GaAs, Cu_2O, diamond, CdTe, ZnTe, and NiO or with p-type organic materials. Different designs for n-ZnO based hybrid single and double heterostructure LEDs have been reported in literature such as:

(i) Reversed p-ZnO/n-GaN based LED
(ii) n-ZnO/p-GaN based LED
(iii) MgZnO/ZnO/AlGaN/GaN double heterostructure LED
(iv) n-ZnO/p-AlGaN single heterostructure LED
(v) GaN/ZnO/GaN based LED
(vi) n-ZnO/p-SiC single heterostructure LED

These ZnO based LED designs are reported in literature with more detail [23]. Due to spontaneous electric polarization, LEDs with single and double heterostructures have interfacial charges. The interfacial charges have strong influence on LEDs as reported in literature. The performance of the LEDs may reduce due to radiative recombination tunnelling of holes and electrons at the opposite sides of the LED interface [23]. Some problems can affect the performance of ZnO based LEDs like;

1. Extra carrier losses at contacts due to the significant imbalance between the holes and electrons partial currents.
2. Poor control of these devices on the emission spectra.
3. High series resistance of these LEDs is not required for low conduction of the p-doped layers [23].

Due to the large lattice mismatch, ZnO is not suitable for some p-type materials to fabricate heterojunction. It has a strong effect on device performance. ZnO has similar physical properties of p-GaN or pAlGaN, so mostly researcher prefers to fabricate their heterojunctions. For the fabrication of laser and blue light emitting diodes, GaN is already in use. So it would be a better option to fabricate ZnO heterojunction with p-type GaN. ZnO has different similarities with p-type GaN. Some similarities are following

- Similar lattice parameters.
- Similar wurtzite crystal structure.
- Similar band gap of ZnO and GaN (3.37 eV and 3.4 eV respectively)
- The Lattice mismatch is only 1.8%.

The n-ZnO/p-GaN heterojunctions based LEDs can have an imbalance between the partial current of electrons and holes as reported in literature. The

junctions have different mobilities of electron and hole, and have different heights at the heterojunction interface. This phenomena cause the imbalance between the mobilities of electrons and holes [23]. The fabrication of different complex device structures is reported by some researchers. To adjust the device structure, different undoped or insulating layers were inserted between p-GaN layer and n-ZnO nanorods. But addition in these layers has changed the emission spectrum in comparison to simple LEDs. The emission spectra of n-ZnO/p-GaN based LEDs have covered the whole visible spectrum with no other light conversion makes it a strong candidate for white light source. There is a large range of investigated results on the n-ZnO/p-GaN based LEDs emission spectrum stated in the literature. The comprehensive studies of n-ZnO/p-GaN LEDs are still under moot and have a large area of interest. The ZnO nanostructure/p-GaN based LEDs have special interest due to their low cost fabrication. The ZnO nanotubes and nanorods based LEDs have the ability to improve light extraction as reported in literature [40]. Some ZnO nanostructures/p-GaN, ZnO nanorods/p-4H-SiC based Light Emitting Diodes have been fabricated. The EL of these ZnO nanorods/p-GaN LEDs showed in figure 2.5. The values of EL were calculated by a photomultiplier detector at a current of 4 mA in forward bias at room temperature. The EL emission could be easily seen with the naked eye.

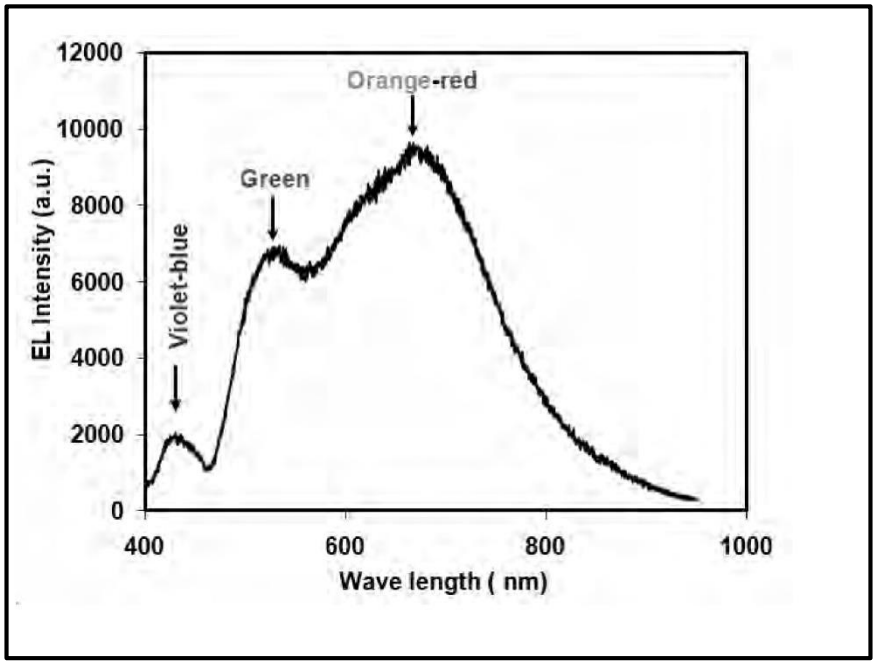

Figure 2.5: The EL of as grown ZnO nanorods/p-GaN heterojunction [40].

The EL spectrum shows three peaks of the developed LEDs which mainly occurred around at 457 nm, 531 nm and 665 nm that are violet-blue emission, green emission and orange-red emission respectively. These emissions are due to deep level defects in the Mg-doped p-type GaN substrate and in ZnO. These can be related to different radiative recombination. Due to the presence of non-radiative recombination centers, the EL emission cannot be sensed at lower injection currents <2 mA. It gives the divert path for the current [40]. These non-radiative recombination centers are saturated at higher injection currents >2 mA. These injected carriers are responsible for the emission of photons due to radiative recombination.

By controlling the crystalline defects in ZnO and by reducing the interface effects, the performance of fabricated devices can be improved. In addition, controlling of defect concentration at the heterojunctions interface is still under moot [40]. The photoluminescence (PL) of ZnO nanorods is shown in Figure 2.6. These PL values were obtained at room temperature. Resonant frequency doubling unit (MBD266) was pumped by a laser diode with laser lines of 256nm wavelength. This unit was used as an excitation source. The observed peaks were at 383 nm, green emission at 553 nm and orange-red emission at 693 nm respectively. The band edge emissions at 383 nm show the free exciton near band edges and good crystallinity of ZnO nanorods.

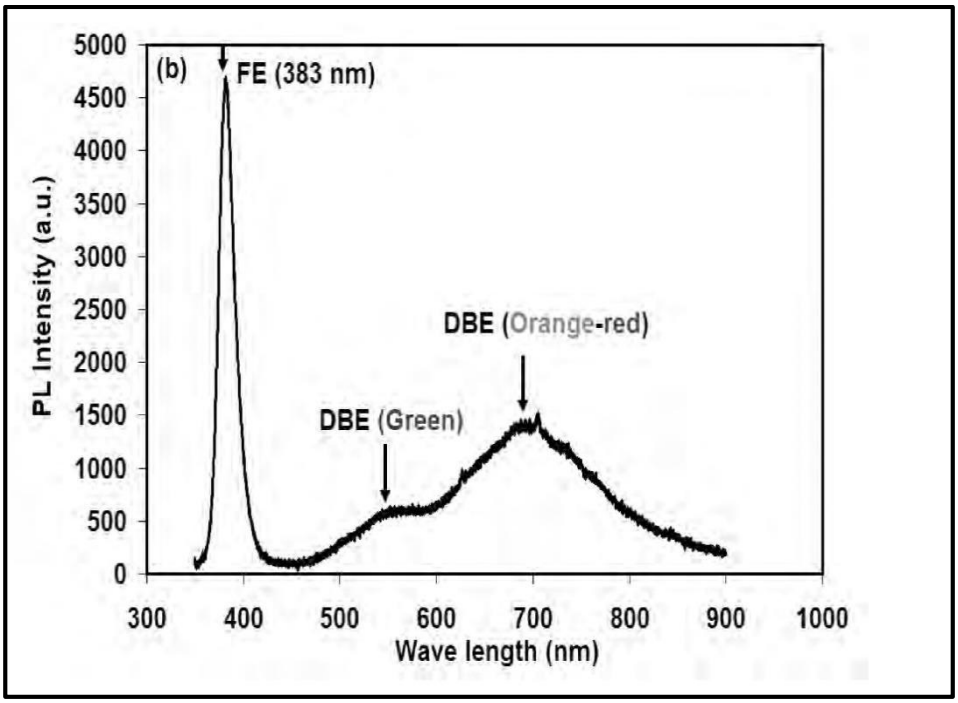

Figure 2.6: Photoluminescence (PL) of the as grown ZnO nanorods/p-GaN heterojunction [40].

The comparison of EL and PL spectrum shows the PL spectrum is constant with the EL spectrum and the PL spectrum does not show the violet-blue peak centered at 457 nm as EL spectra shows that. It can be predicted that this peak is from the heterojunction or from the substrate. The maximum possibility of this peak is from the Mg-doped p-GaN substrate depends on transitions from the shallow donors or conduction band to deep Mg accepters.

So it shows that the combined emissions from the n-ZnO nanorods and the p-GaN form EL emission from developed LEDs. It can also be explained by using figure 2.7 which shows the Anderson model's developed energy band diagram [31]. The electron affinities (χ) and band gap energies (E_g) of both ZnO and GaN are 4.35 e V, 4.2 e V and 3.37 e V, 3.4 e V, respectively. These values were used for construction of band diagram.

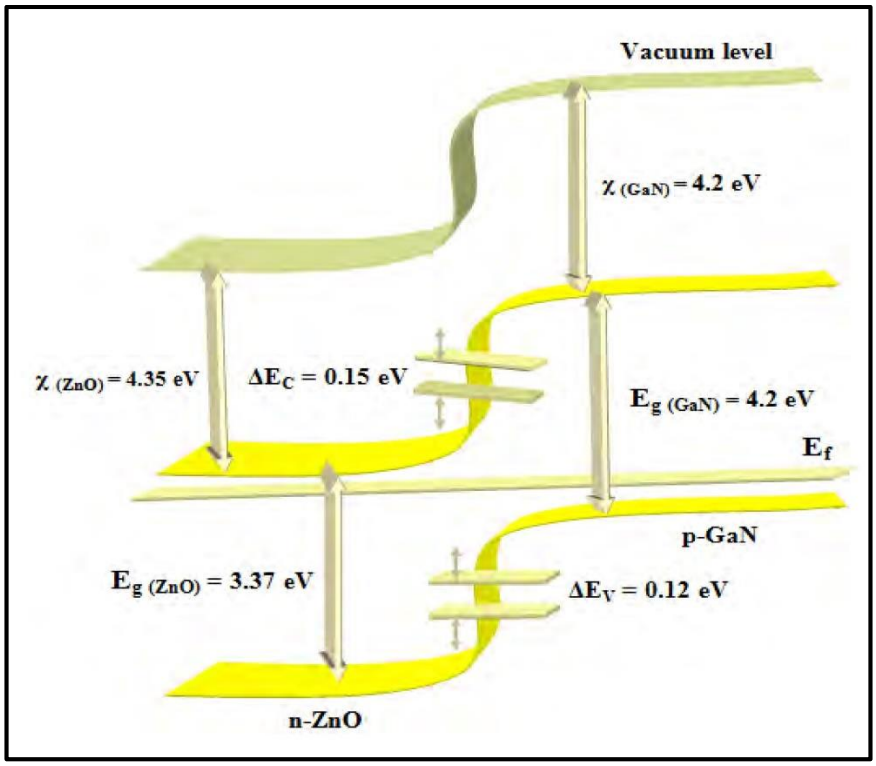

Figure 2.7: n-ZnO/p-GaN heterojunction structure Energy band diagram developed by Anderson model [46].

The energy band diagram shows holes energy barrier:

$$\Delta EV = Eg\,(ZnO) + \Delta EC - Eg\,(GaN)$$

$$3.37 + 0.15 - 3.4 = 0.12\,eV$$

And electrons have:

$$\Delta EC = \chi\,(ZnO) - \chi\,(GaN)$$

$$4.35 - 4.2 = 0.15\,eV$$

This shows the same energy barrier for electrons and holes approximately [40].

The formation of non-radiative centers at the interface decreased the efficiency of the ZnO film/p-GaN based LEDs as reported in literature and a wide band gap MgO has been added into ZnO film/p-GaN LEDs to increase efficiency of LEDs. For further improvement in the efficiency of the LEDs, an intermediate layer of AlN is introduced into ZnO film/p-GaN LEDs. AlN has the excellent chemical and physical properties with largest direct band gap of 6.2 eV in III-nitride semiconductors [47].

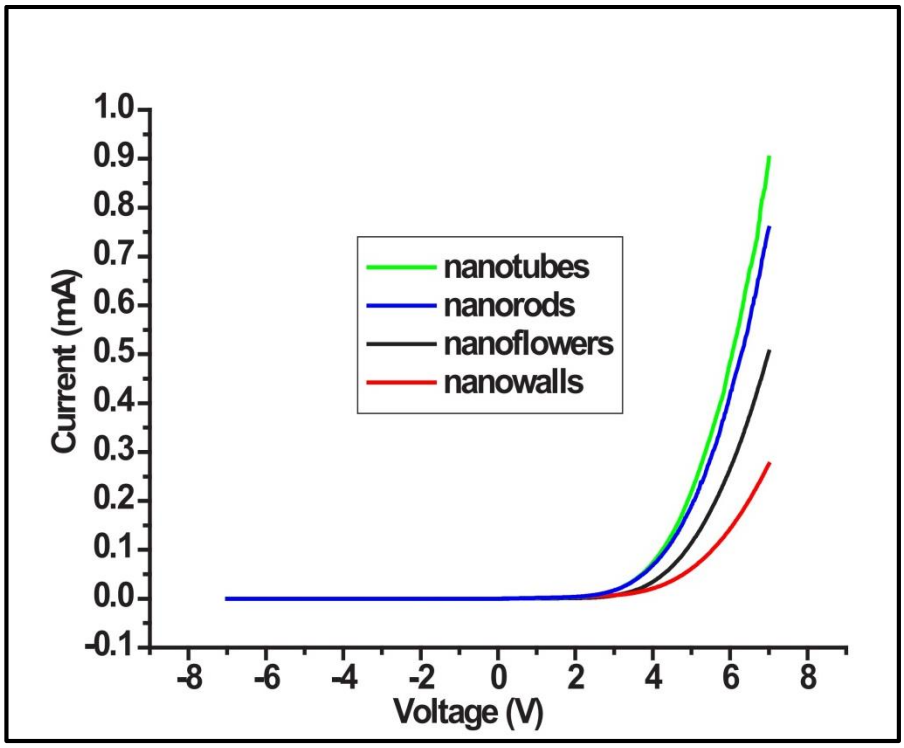

Figure 2.8: I-V curves for different ZnO (nanostructures) /p-GaN LEDs [16]

Figure 2.8 shows the excellent I-V characteristics of n-ZnO (nanostructures) /p-GaN based LEDs [16]. All LED devices show expected rectifying behavior. It shows the reasonable p-n heterojunction between the n-ZnO nanostructures/p-GaN substrate. These fabricated heterojunctions LEDs have the turn-on voltage around 4 V [16].

Figure 2.9 shows the CIE 1931 color space chromaticity diagram in the coordinate system of (x, y) for the n-ZnO nanostructures/p-GaN based LEDs [16]. The chromaticity coordinates are close to the Planckian locus (about > 1 MacAdam ellipse away) for n-ZnO nanowalls and nanoflowers. It confirmed that the LEDs according to the US standard ANSI_ANSLG C78, 377-2008 for solid state light sources. According to this standard, the only light sources can produce white light which has the coordinates of chromaticity within three MacAdam ellipses from the Planckian locus. The nanorods and nanotubes based LEDs are away from Planckian locus more than three MacAdam ellipses. So these cannot be considered white light, but too close to white light.

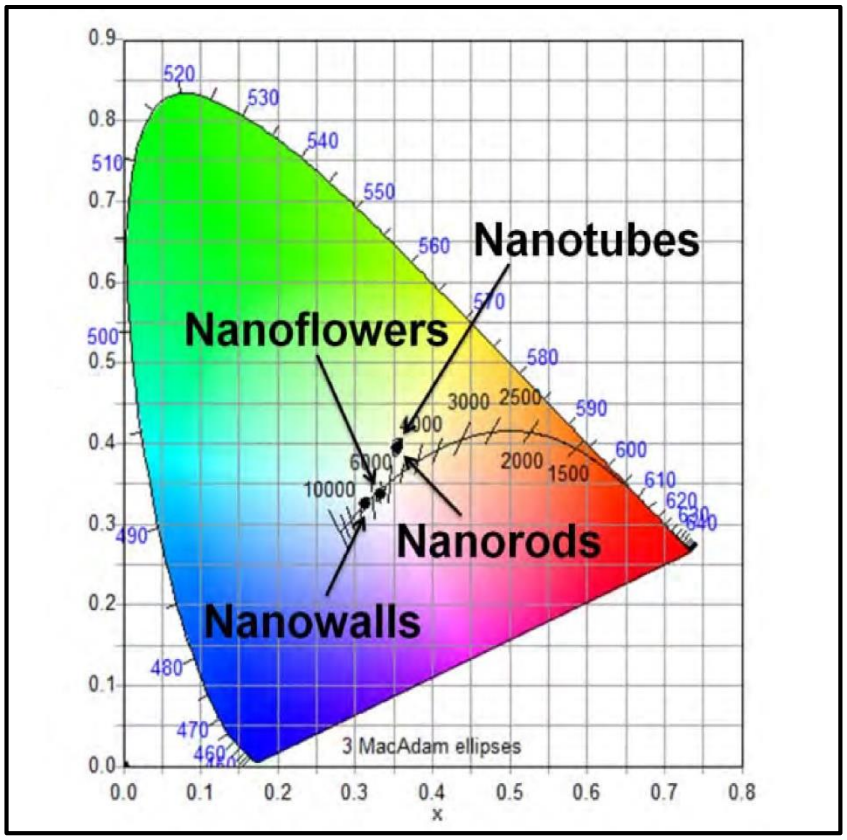

Figure 2.9: The CIE 1931 color space chromaticity diagram of ZnO nanostructures based LEDs [16]

2.2.3. ZnO based Biosensors

Recently, ZnO has become very attractive material for the production of biosensors. Due to the high bio-safety and non-toxicity, many research groups are using ZnO in bio-sensing field. It is electro-chemically active and its nanostructure can grow easily and economically. So ZnO becomes attractive material for detection of different biological molecules due to its promising properties. ZnO nanostructures are on emerging stage for the use in biosensors, so very less data is reported [36]. In frog oocytes and human adipocytes, a selective intracellular glucose sensor was used to measure the glucose concentration. This glucose sensor was fabricated by the growth of ZnO nanoflakes on the borosilicate glass capillary tip.

By uricase immobilization on ZnO nanowires, a reproducible and stable potentiometric uric acid biosensor were fabricated [36]. Figure 2.11 (a, b) showed the uric acid biosensor time response at 100 µM and the figure 2.11 (c, d) showed the calibration curves with membrane and without membrane for the sensor. The response time of the sensor increased from 6.25 s to > 9 s by applying nafion membrane. It also increased the linear range from 1µM to 1000 µM. The sensor

stability also increased by applying the membrane. The measurements showed that the sensor response was not affected by normal concentrations of common interferents [36].

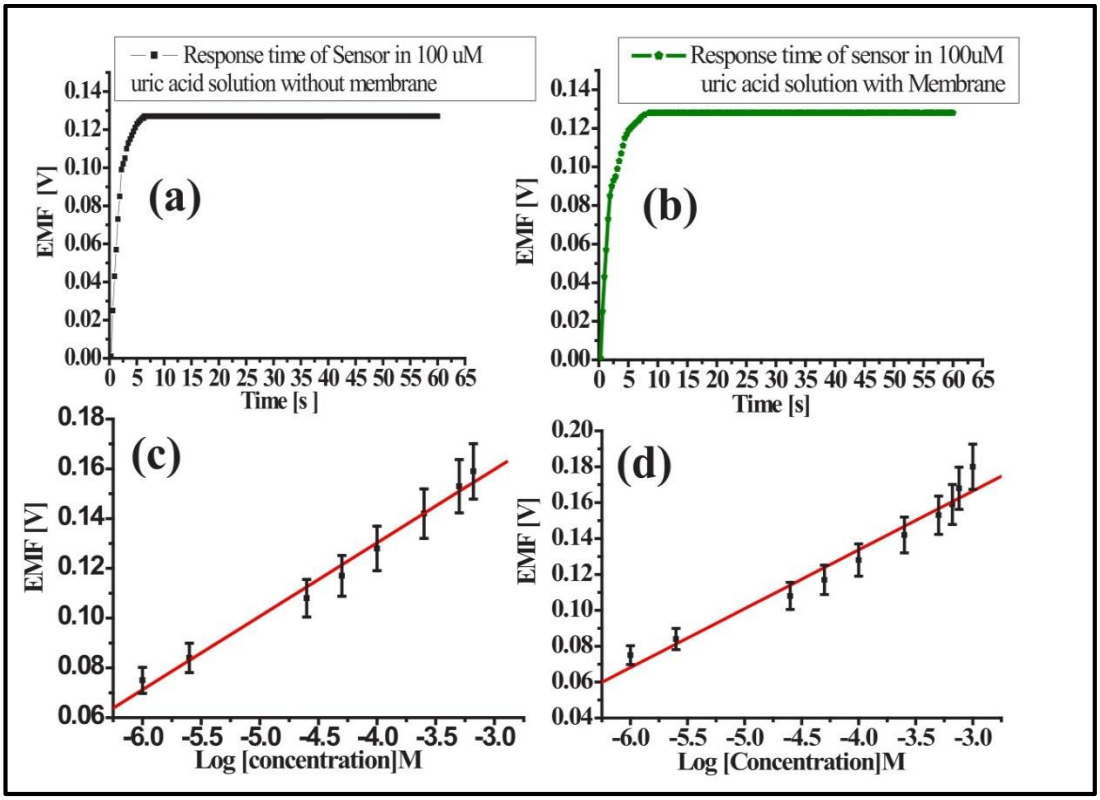

Figure 2.10: ZnO nanowires/Uricase sensor electrodes time response at 100 µM uricacid solution (a) without membrane (b) with membrane. The uric acid sensor's calibration curves (c) with membrane (d) without membrane [21].

3. Experimental Work

The multiple range of ZnO nanostructures makes it a unique material for the use in different applications, such as electronics, sensing, optoelectronics etc. These nanostructures can easily form in a versatile variety like nanotubes, nanorods, nanowalls, nanobelts, nanorings, nanoflowers, nanowires, nanohelixes, nanocages, and nanosprings. Different methodologies are in use for the synthesis of these nanostructures such as electro-chemical deposition (ECD), vapor-liquid-solid (VLS), aqueous chemical growth (ACG), chemical vapor deposition (CVD), chemical vapor transport and condensation (CVTC), physical vapor deposition (PVD) and metal organic chemical vapor deposition (MOCVD) [48-53]. The surface of different p-type substrates are being used to grow ZnO nanostructures. This research work consists of two basic parts, i.e. the growth of one dimensional ZnO nanostructures and the final device fabrication. Figure 3.1 shows the schematic of device fabrication. It includes the (1) basic preparation of substrate, (2) growth of one-dimensional nanorods, (3) deposition of bottom contacts, (4) photo-resist spinning and (5) deposition of top contacts.

3.1. Growth of One-Dimensional ZnO Nanostructures

The growth of one-dimensional nanostructures with chemical bath deposition has two basic parts, i.e. the pre-treatment of the substrate and then final growth of the nanostructure. Pre-treatment includes the cleaning of substrate with different methods such as washing with diluted HF and sonication in ethanol, etc. In the second step, pre-treated substrate is placed in growth solution for final growth of the nanostructure.

3.1.1. Substrate Pre-Treatment

To achieve high quality and well aligned growth of the nanostructure, substrate pre-treatment is very essential. Commercially available substrates have different dust particles, oxide layers and chemicals on their surfaces. Different methods were used to clean these particles from the surface of substrate. Both simple rinsing and sonication did not produce acceptable morphology of nanostructures so treatment with a solution which can dissolve the top layer was tried. These kinds of

solution are usually acids and use of acids needs special precautions. Hydrofluoric acid (HF) is a recommended solvent for SiO_2 film on Si substrate and oxide layer on GaN substrate. HF is a very hazardous acid, so it was used with acetic acid in a ratio 3:1 (acetic acid: HF). When the substrates were just dipped in this solution, complete oxide layer got removed from the substrate and dissolved in the solution. So the solution was diluted further as 9:1 (de-ionized water: solution). Now on dipping of substrates the oxide film did not detach from the substrates and dipping was done for two minutes only. The substrates were also washed with DI-water during these steps. Later the substrates were sonicated in pure ethanol for 15 minutes and this procedure was repeated for acetone as well. At the end, the samples were dried after the several times washing with DI-water.

3.1.2. Growth of ZnO Nanorods by Chemical Bath Deposition

Vayssieres et al. introduced a simple method to grow the ZnO nanorods. This technique has the low temperature (<100 C) process for the growth of nanorods. The solution of two basic chemicals, i.e. zinc nitrate (Zn $(NO_3)_2$ $6H_2O$) with hexamethylenetetramine (HMT, $C_6H_{12}N_4$) is used for the growth. The concentrations of HMT and zinc nitrate (0.010 - 0.075 mM) were maintained. Pre-treated substrate was placed in growth solution with upside down towards the bottom of the beaker and kept the beaker in an oven at 60- 95 ºC for 2-5 hours. The reactions that take place in solution for the growth of nanorods are described below [54].

In the first step, ammonia was produced in reaction of water with HMT:

$$C_6H_{12}N_4 + 6H_2O \rightarrow 6HCHO + 4NH_3$$

Further the water reacted with already produced ammonia and splits into ammonium and hydroxide ions as follow:

$$NH_3 + H_2O \rightarrow NH_4 + OH^-$$

The solid ZnO nanorods grow on the substrate by the reaction of hydroxide ions with zinc ions by following reaction below:

$$2OH^- + Zn^{2+} \rightarrow ZnO(s) + H_2O$$

Then the sample was removed from the growth solution and washed in de-ionized water. By using the above method, the grown ZnO nanorods have less density and alignment. To get the high density and well aligned ZnO nanorods, enhanced method by combining the growth process with substrate preparation technique (deposition of seed layer) i.e. calling the two step chemical bath deposition

was used. Greene et al. reported this method [55]. The details of the process used in this research work are as follows:

3.1.2.1.1. Deposition of Seed Layer

The solution of 5mM concentration of zinc acetate dehydrate (Zn $(OOCCH_3)_2.2H_2O$) was dissolved in ethanol to prepare the seed solution. Seed solution was stirred for 30 minutes on a hot plate at 60 °C. The stirring speed was 300 rpm. The deposition of the seed solution was performed on the substrate using a spin coater with 1800 rpms for 30 seconds. This process was repeated for 3 to 4 times to cover the whole surface of the substrate in order to improve the uniform coverage of seed. Presence of seed layer on the substrate was confirmed using atomic force microscope (AFM).

3.1.2.1.2. Annealing of Substrates

Further the coated substrates with seed layers were kept in the muffle furnace to remove the moistures and to get the strong adhesion of the thin layer with substrate. These substrates were annealed at 250 °C for 30 minutes in a muffle furnace.

3.1.2.1.3. Growth Process of Nanorods

The aqueous solution of zinc nitrate (Zn $(NO_3)_2$ $6H_2O$) with hexamethylenetetramine (HMT,$C_6H_{12}N_4$) solutions were prepared. The concentration of the aqueous solutions of both chemicals was kept to 0.1 M. Both solutions were prepared separately and then mixed together in a beaker. Then pre-treated substrates were mounted in Teflon bar to the growth side down towards the bottom of the beaker. The substrates were inclined in the solution around the angle of 70º for the perfect growth. To avoid contamination, the beaker covered with aluminium foil. Then the beaker was placed in the oven for 2.5 hours at 93-95 °C. The substrates were removed from the Teflon bar after completing the growth process and rinsed with DI-water to wash the substrates and dried.

3.2. Device fabrication

3.2.1. Bottom Contacts Deposition

The structure of metallization patterns with low contact resistance of ZnO nanostructured based devices makes them more stable and reliable. The electrical and electro-optical characteristics of a device are totally dependent on the low resistant contacts between a metal and semiconductor. It has also a strong impact on device performance and its life time [56]. Electrical devices use ohmic contacts to transfer electrical current through them.

Table 3.1: Design of different ohmic contacts for p-GaN

Metallization Scheme	Annealing Temp.	Lowest Resistant Contacts $\rho_c\,(\Omega\text{-}\,cm^{-2})$	Reference
Pt/Au	750°C	1.5×10^{-3}	49
Ni/Au	750°C	3.3×10^{-2}	49
Pd/Au	500°C	4.3×10^{-4}	48
Pt/Ni/Au	350°C	5.1×10^{-4}	52
Ni/Pd/Au	550°C	4.5×10^{-6}	50
Pd/Ni/Au	450°C	5.1×10^{-4}	53
Pd/Pt/Au	600°C	5.5×10^{-4}	51
Ni/Au	500°C	5.1×10^{-4}	53

Ideally the ohmic contacts should have linear and symmetric I-V characteristic. We used different metal alloys in our research work for the fabrication of the bottom contacts to the p type substrates.

Table 3.2: Design of different ohmic contacts for n-ZnO

Metallization Designs	Annealing Temp.	Lowest Resistant Contacts ρ_c (Ω- cm^{-2})	Reference
Ti/Au	300°C	$2.0x10^{-4}$	57,58
Ti/Al/Pt/Au	200°C	$3.9x10^{-7}$	55,56
Ti/Au	600°C	$3.0x10^{-3}$	59
Ti/Al/Pt/Au	None	$8.0x10^{-7}$	55,56
Ti/Au	None	$4.3x10^{-5}$	60
Zn/Au	500°C	$2.36x10^{-5}$	63
Pt-Ga	None	$3.1x10^{-4}$	67
Al	None	$4.0x10^{-4}$	61
Ru	700°C	$3.2x10^{-5}$	66
Al/Pt	None	$2.0x10^{-6}$	61,62
Re/Ti/Au	700°C	$1.7x10^{-7}$	65

The Ni/Au alloy was used for GaN. The thickness of Au and Ni layers were 20 nm and 20nm, respectively. Then the sample was annealed under the atmosphere of nitrogen (N_2/Ar) gas at 650°C for 1 min. The minimum expected contacts resistance of this alloy is 5.1×10^{-4} Ω-cm^{-2}. Table 3.1 shows the different ohmic contact patterns for the p-GaN. For p-GaN substrates, an Al layer with thickness of 150 nm was used to develop ohmic contact.

3.2.2. Photoresists Coating

Nanorods have small spaces between each other. So we used an insulating photo-resist layer to fill these spaces. This layer also cuts off the connection of top contact with a p - type substrate at the bottom of nanorods. Spin coating was used to deposit this layer on ZnO nanorods. It also avoided the crossing of carriers between nanorods. The insulating photo-resist layer also covered the top surface of nanorods.

3.2.3. Top Contacts Deposition

The ohmic contacts to ZnO nanorods were fabricated by the deposition of non-alloyed Ti/Au metal system. Ti and Au layers have the thickness of 20 and 20

nm, respectively. The minimum specific contact resistance of this non alloy contact is 1.2×10^{-5} Ω -cm^{-2} [57]. Table 3.2 shows the different designs of ohmic contacts for n- ZnO.

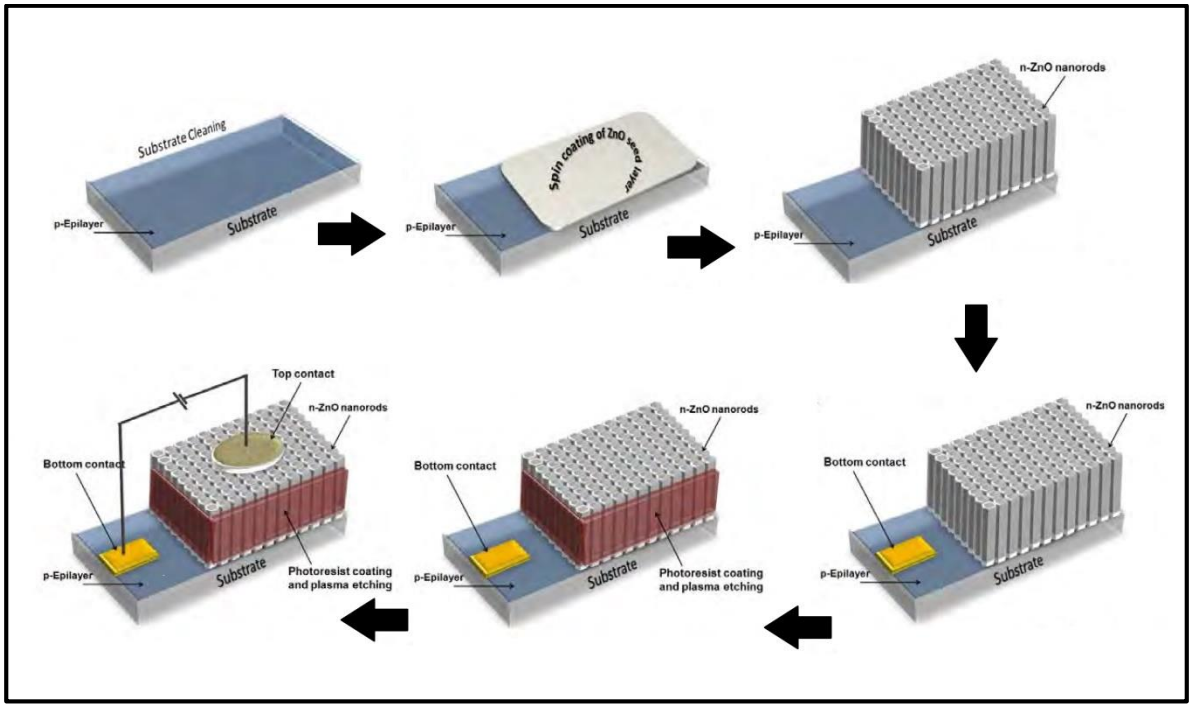

Figure 3.1: Schematic for the device fabrication.

4. Characterization Tools

We used the following characterization tools to investigate the, morphological, optical, electrical and electro-optical properties of ZnO and final fabricated device in our research work.

a) Atomic Force Microscopy (AFM)
b) Scanning Electron Microscope (SEM)
c) X-ray Diffraction (XRD)
d) UV-Visible Spectroscopy
e) Fourier Transform Infrared Spectroscopy
f) Photoluminescence (PL)
g) Electroluminescence (EL)

4.1. Atomic Force Microscopy (AFM)

Atomic Force Microscopy is used to investigate the surface topography. It measured the force between its tip and surface of sample to investigate the topography [58]. The topographical images produced by the deflection of the tip cantilever while scanning the surface of the sample. Tip deflection is due to the repletion between the tip and surface by Van der Waals forces. The deflection is detected by the reflection a laser off the cantilever onto the photodiode array. Then this detected deflection is used to produce an image. AFM used three modes of scanning for the measurement.

I. Contact Mode
II. Non-contact Mode
III. Tapping Mode.

The tip is in contact with the surface during scanning the surface in contact mode. While in non-contact mode, tip fluctuates a few nanometers above the surface due to Van der Waals forces. The scanning can also be done by keeping the constant fluctuation of frequency or amplitude, and moving the tip to compensate. The tip and sample are not dragged in non-contact mode due the friction between them.

In tapping mode, both contact and non-contact scanning occurred. The tip has the highest value of fluctuation in tapping mode than the non-contact mode so it can make the both scanning modes (contact and non-contact mode) with the surface of the sample. This mode can also be used to control the contaminations like the water adsorbed on the surface of the sample while the tip and sample damage limited. Atomic Force Microscopy doesn't require any sample preparations and measurements can be done at room temperature.

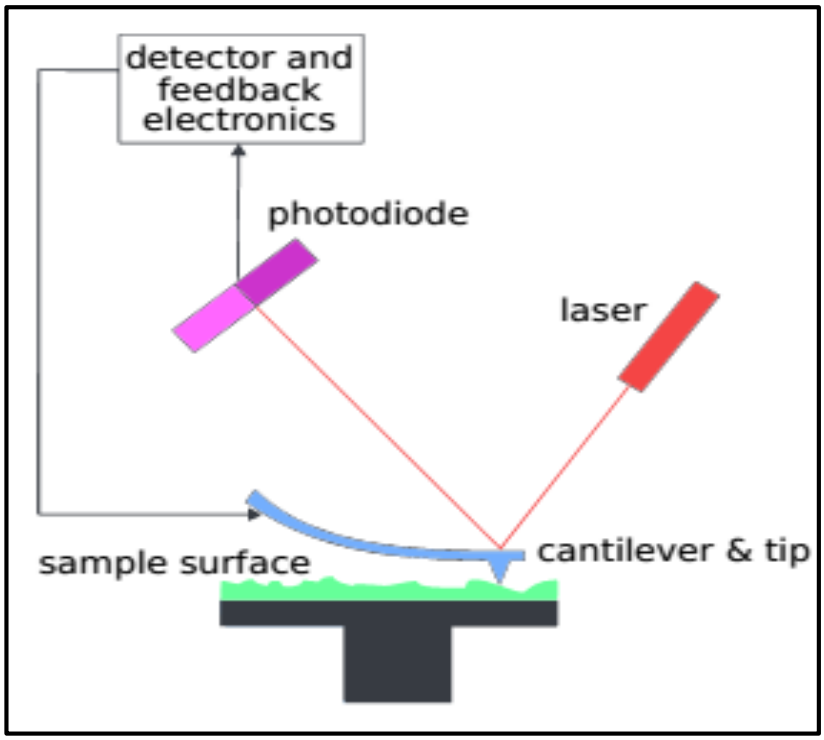

Figure 4.1: Schematic of an AFM.

4.2. Scanning Electron Microscope (SEM)

Scanning Electron Microscope is a microscope which uses electrons to measure the surface topography or sample composition instead of light or AFM tip. An electron beam generates with an electron gun which is accelerated by the wire grids with positive charges. The magnetic and electrostatic lens is used to focus this beam on the sample surface. While scanning on the surface of a sample, low energy electrons also known as secondary electron scatters in-elastically from the surface and detected by the detector. Scanning electron microscope uses the signal from these low energy electrons to produce the image of the scanning surface. Because these low energy electrons escapes within few nanometers of the sample surface.

Scanning electron microscope used different detectors to produce the results by detecting backscattered electrons and x-rays.

Small electron beams can be used for large depth of field to produce high resolution images. It can also investigate the structures with high-aspect-ratio. Scanning electron microscope requires a high vacuum chamber to perform scanning. Samples must be conductive. Insulators are coated with conductive layers before the scanning to avoid charging. Because this charging can be introduced the artifacts in surface images [59]. Fig 4.2 shows the schematic of an SEM.

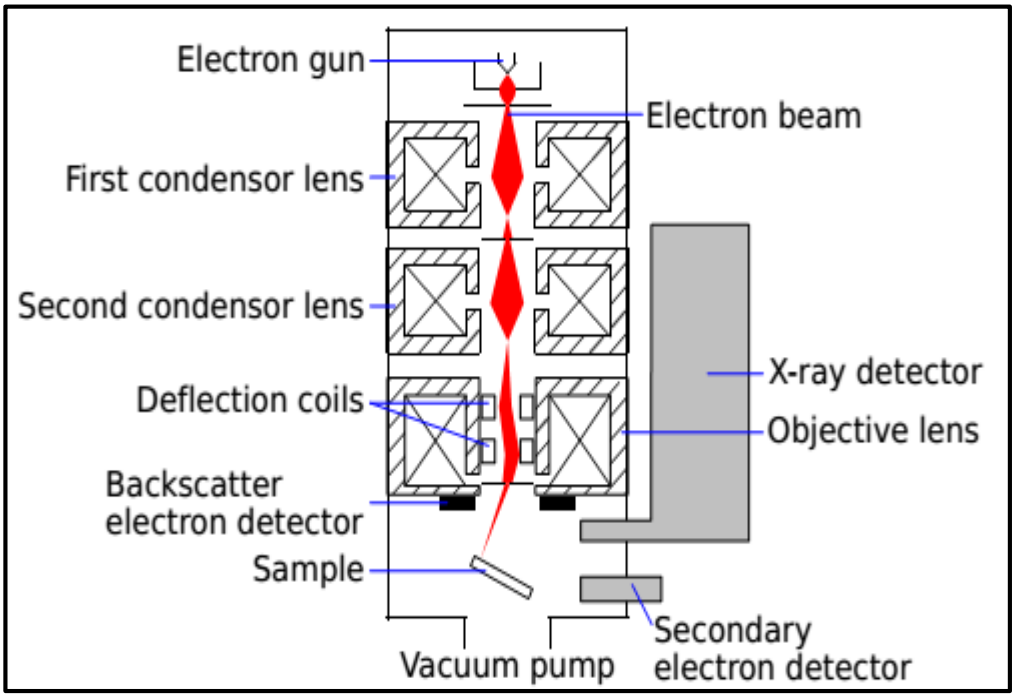

Figure 4.2: Schematic of a SEM.

4.3. X-ray Diffraction (XRD)

The crystallographic structure of a material can be investigated by using x-ray diffraction (XRD) measurements. In these measurements, X-rays falls on the surface of the sample and scatter off the electrons elastically from the atom. If it runs into a periodic array of atoms, the scattered waves will reinforce in certain directions and cancel in others. So a crystal is made up of families of lattice planes and only strong X-rays reflected by each plane arrive at the detector in phase, which makes them ideal to explore structural details of crystals [60]. Diffraction occurs on the principle of Bragg‘s law which is stated below

$$2d \sin(\theta) = n\lambda$$

Where the inner planes spacing are ‘d’, ‘θ’ is the incident angle, the wavelength of x-ray is ‘λ’ and ‘n’ is order. The schematic is shown in Figure 4.3

For hexagonal crystal structure like ZnO, the plane equation is

$$\frac{1}{d^2} = \frac{4}{3}\left(\frac{h^2 + hk + k^2}{a^2}\right) + \frac{l^2}{c^2}$$

By combining it with Bragg’s law, the equation will be

$$\sin^2\theta = \frac{\lambda^2}{4}\left[\frac{4}{3}\left(\frac{h^2 + hk + k^2}{a^2}\right) + \frac{l^2}{c^2}\right]$$

Where lattice parameters are ‘a’ and ‘c’, the miller indices are ‘h’, ‘k’, ‘l’ and plane spacing is shown of ‘d’. The crystallite size can be measured by using Scherrer equation.

$$D = \frac{k\lambda}{\Delta\theta}$$

Where crystallite size ‘D’, wavelength ‘λ’, ‘θ’ is angle, ‘Δ’ is peak breadth and ‘κ’ is Scherrer constant. Scherrer constant depends on the crystalline shape, size and peak breadth. For this study XRD analysis was carried out using STOE powder diffractometer at SCME NUST. It utilizes a monochromatic radiation Cu Kα with wavelength of 1.54 Å. The scan range was selected between of 30° to 80° with step size of 0.04 and stay time at each step of 1 sec. Software named as ‘X-pert Highscore Plus’ was used to get information about the type and amount of phases present.

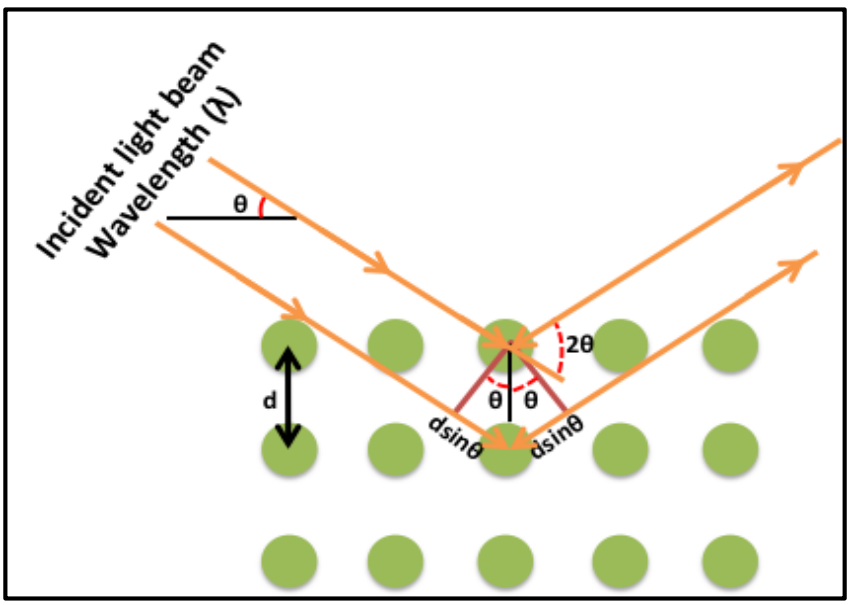

Figure 4.3: X-rays diffraction from Crystal Structure.

4.4. UV-Visible Spectroscopy

An ultraviolet-visible spectroscopy is used to measure the light in the ultraviolet region, visible region and near infrared region. An electromagnetic (light) energy is transmitted to sample atoms, ions, or molecules. Transition to a higher energy state occurred. The transition can be change in electronic levels, vibrations, rotations, translation, etc. According to the Beer's law, the amount of light absorbed by a sample is dependent on the path length, concentration of the sample and the proportionality constant. The Beer's Law is

$$\boldsymbol{A = \varepsilon bc}$$

Where 'A' is the amount of light absorbed, 'b' is path length, concentration of the sample is 'c' and 'ε' is a proportionality constant. So by measuring absorbance or percent transmittance at a given frequency gives information related to the amount of sample concentration present with an identified ε and λ. The components of UV-Vis spectrometer depends on four basic parts which are a light source, λ selector, sample cell holder, detector (amplifier, recorder). Figure 4.4 shows the basic schematic of UV-Vis spectrometer.

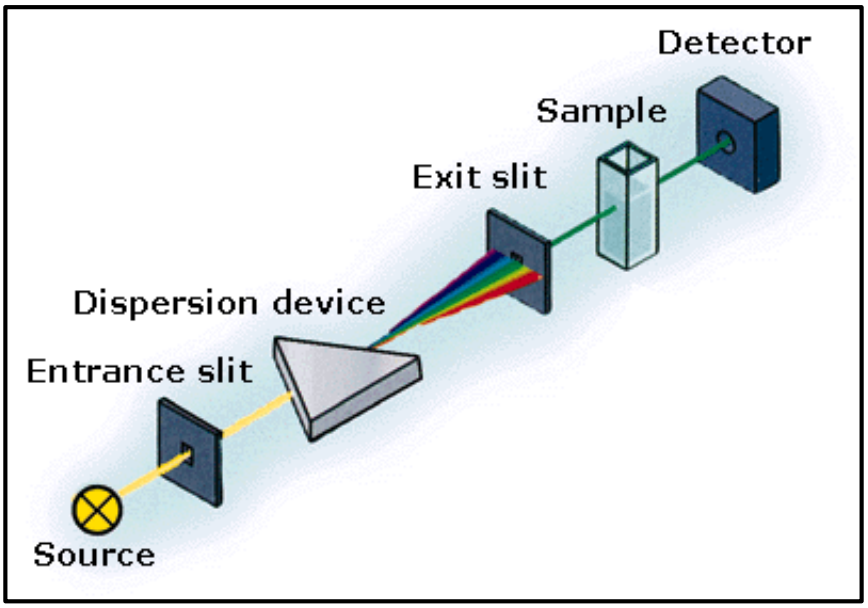

Figure 4.4: Schematic of UV-Vis Spectrometer.

4.5. Fourier Transforms Infrared Spectroscopy

FTIR is used to compare and identify the unknown particulate and materials. In addition, it is also used in different investigations related to coatings, defects, compositional differences and polymer heterogeneity. It used infrared light

to identify different chemical bonds in the sample material. It has the molecular fingerprint spectra of the pure compounds, simple for inorganic, very rich and detailed spectra of organic compounds. Different materials have the different molecular bond vibrations at different frequencies. The molecular bonds absorb different frequencies of light energy for transition from the lower energy state of high energy state. This cause the vibration in bonds and the frequency require for this transition is equal to the difference in stable state and excited state energies.

The energy difference in the two states = absorbed energy by bonds

$$E_1 - E_0 = hc/\lambda$$

Where the Planck's constant 'h', light velocity is 'c' and λ is the light wavelength.

The energy required for the transitions in molecular vibrational states is 1-10 kilocalories/mole which is in the range of the infrared spectrum. The schematic of an IR spectrometer is shown in figure 4.6.

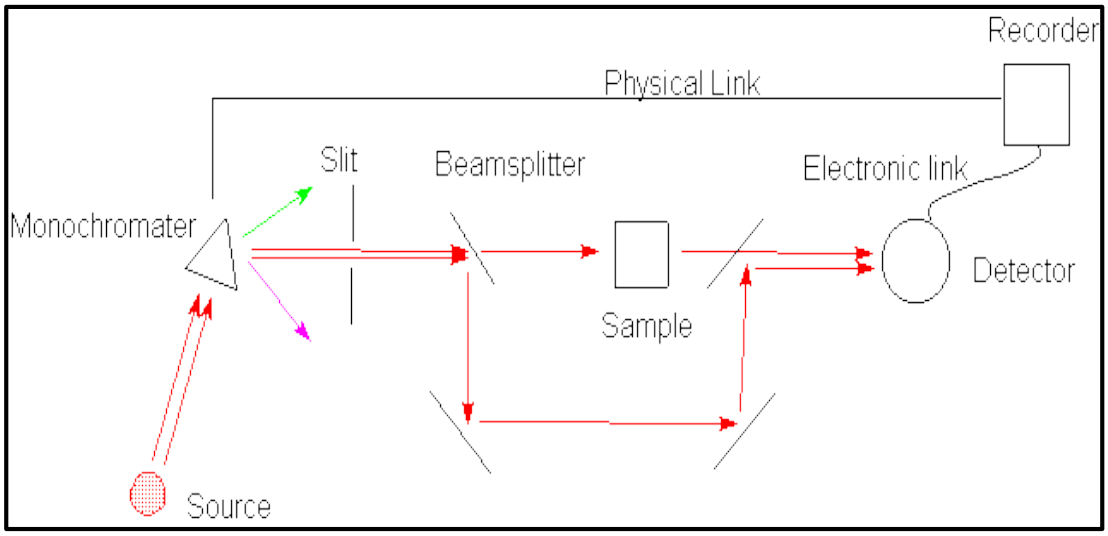

Figure 4.5: Schematic of an Infrared Spectrometer.

4.6. Photoluminescence (PL)

The intrinsic and extrinsic properties of a material can be investigated by the Photoluminescence (PL). In this technique, a semiconductor excites optically, which result the impulsive emission from the radiative recombination in the band gap. Both radiative and non-radiative recombination occurred in the PL process. We used radiative recombination only. We can investigate the impurity level, bandgap, defects detection and recombination processes by using this PL technique [61].

Figure 4.6 shows the schematic of a PL. The PL has three main steps to investigate a material.

1. Electron-hole pairs generated by optical excitation of semiconductor.
2. Spontaneous emission due to electron-hole pair radiative recombination.
3. Finally the emitted light spread by double grating monochromatic is detected by photomultiplier detectors and computer shows the final analysed spectrum.

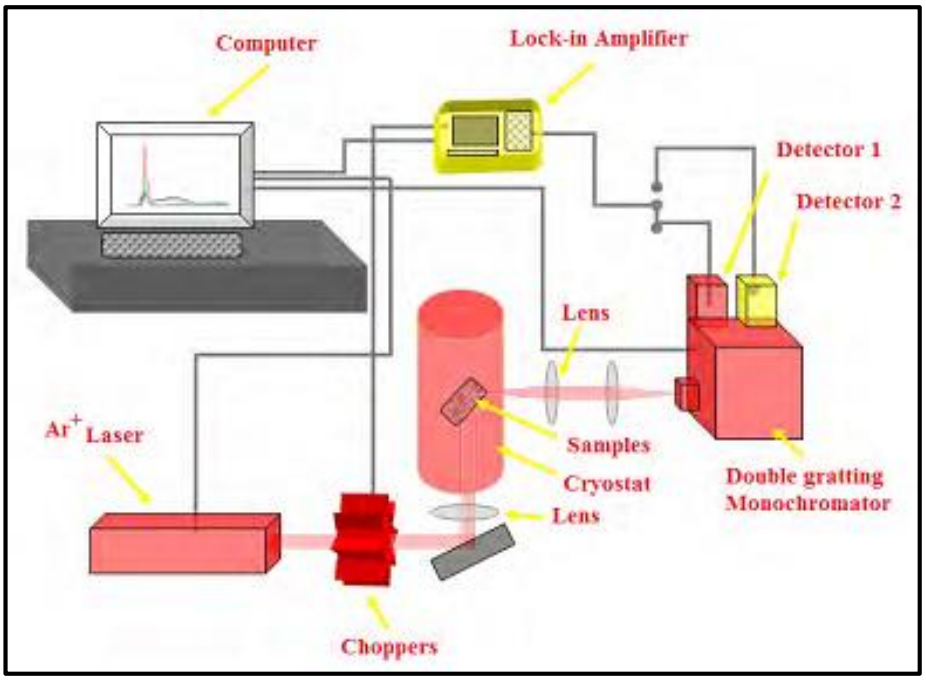

Figure 4.6: Schematic of a PL setup.

4.7. Electroluminescence

The electroluminescence is used to investigate the electro-optical phenomenon of materials. A semiconductor material shows the emission spectrum when an electrical current passes through the material. This is due to the radiative recombination of the electron-hole pairs. The EL is directly related to the efficiency of LEDs. The efficiency of LEDs can be improved by improving EL. Different factors affect the efficiency of LEDs such as injection, transport and recombination of carriers charge. When a forward biased current passes through the heterojunction of an LED, it emits the light which is detected by the photomultiplier detector. This light emission can be detected at the top contact of the LEDs because it escapes from the top edge contact of the electrode [62].

5. Results and Discussion

The different results are obtained by using different characterization techniques. The results showed different effects on the synthesized ZnO nanorods. All the results are discussed below.

5.1. Effect of Parameters

The effect of varied parameters is divided into two main parts. The first part shows the effect of different seed layer parameters of the final growth of ZnO nanorods and second part showing the effect of growth parameters on the grown ZnO nanorods.

5.1.1. Effect of different Seed Layer Parameters

The effect of different seed layer parameters was studied such as the thickness of seed layer on the substrate and spin coating speed to deposit the seed layer on the substrate.

5.1.1.1. Thickness of Seed layer

The increasing concentration of seeds on the substrate highly affects the final growth of ZnO nanorods. Different numbers of drops were studied while the other parameters were kept constant for the whole investigation, such as the speed of spin coater was set on 1800 rpm, the coating time was 30 sec for each drop, the quantity for each drop were 10 µl and the annealing time for the seed layer was 30 mins at 250 °C.

Firstly, the effect of 3 drops was investigated. Only 3drops were coated on a substrate using spin coating. It shows the random distribution of seeds on the surface of substrate and similarly it affects the distribution of ZnO nanorods. The SEM images give the evidence of this effect in figure 5.1 (a, b). The figure 5.1 (a) is showing that concentrations of seeds were less on the substrate which affected the distribution of final grown ZnO Nanorods.

Secondly, 5 drops were deposited on the substrate. The distribution of ZnO nanorods covered the whole area of substrate and showed the uniform growth of ZnO nanorods. The well oriented and uniform distribution of ZnO nanorods can be seen in

figure 5.1 (d). Figure 5.1 (c) shows the enough concentration of seeds on the surface of substrate.

.

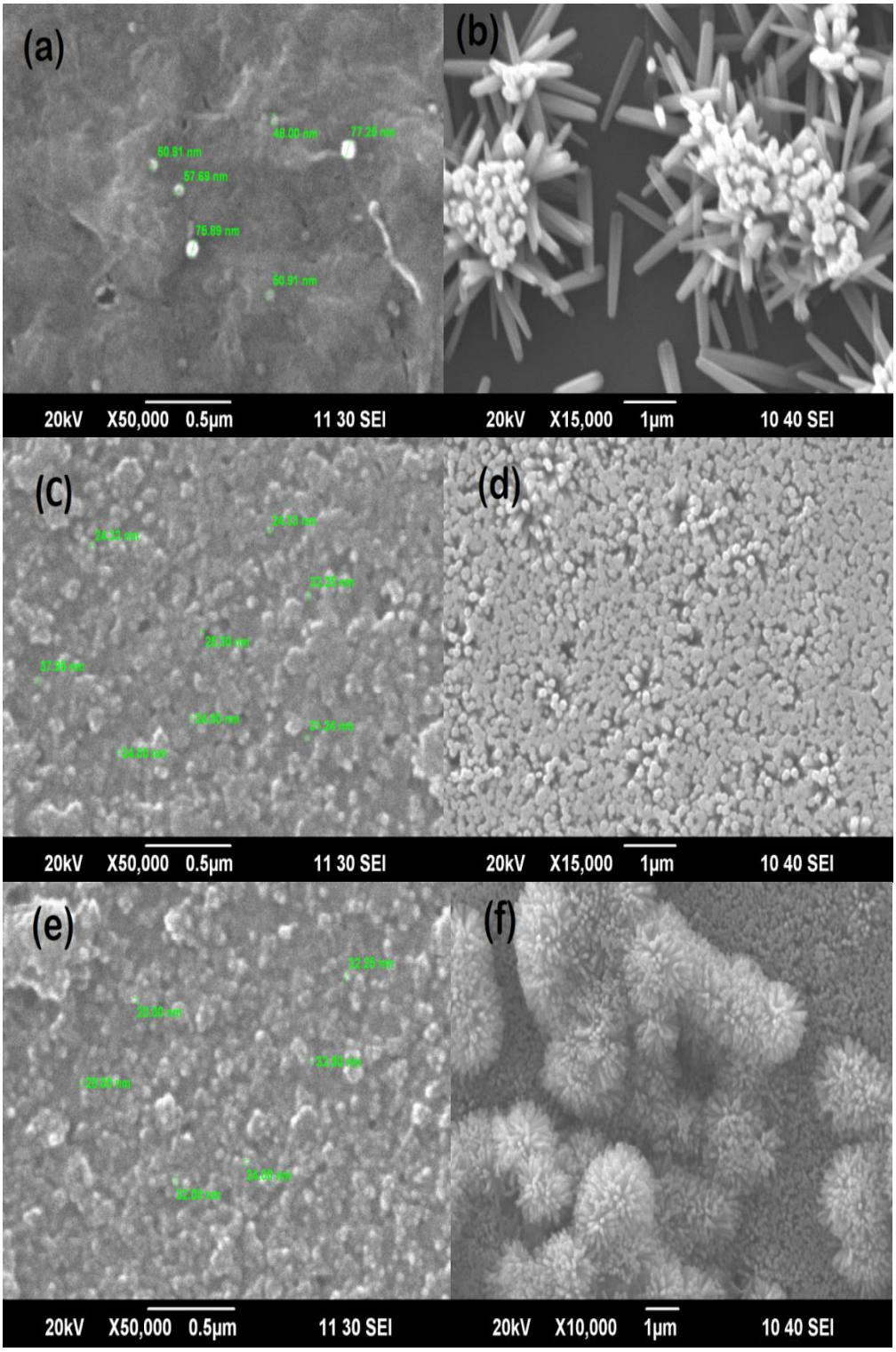

Figure 5.1: Seeds concentration effect at 30µl (a, b), 50µl (c, d) and 70µl (e, f) respectively.

The concentrations of seeds were increased by depositing 7 drops on the substrate. Figure 5.1 (e, f) showing the concentration of seeds on the substrate and the finally grown ZnO nanorods. It is clearly seen that the concentration of seeds increased as compared to previous concentrations. With the increasing concentration, the seeds started depositing on the previously deposited seeds. So the finally grown ZnO nanorods also start to grow in the manner as figure 5.1 (f) showing the flower like shapes of ZnO nanorods on the nanorods grown at bottom of the substrate.

The concentration of seeds on the surface of the substrate can also be observed by the AFM results. Figure 5.2 (a, b, c) is showing the increasing concentrations of seeds on the substrate surface with increasing the amount of solution by 30 µl, 50 µl and 70 µl respectively.

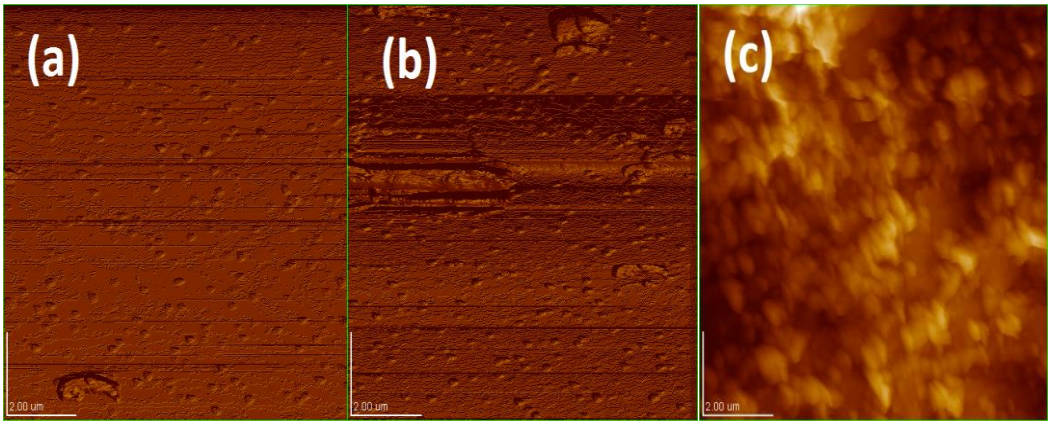

Figure 5.2 (a, b, c): The increasing concentration of seeds with increasing seed solution by 30µl, 50µl and 70µl respectively.

5.1.1.2. Speed of Spin Coater

A spin coater was used to deposit the seed solution on the substrate surface. The speed of the spin coater highly effected the ZnO nanorods distribution on the substrate. It was observed that the substrate coated with low rpm coating speed has the highest distribution of ZnO nanorods as compared to the substrate coated with high rpm coating speed. Different rpm speeds were used to investigate the distribution of ZnO nanorods. Figure 5.3 shows the effect on both seeds and ZnO nanorods distribution.

Firstly the seed solution was deposited on the substrate by spin coating at 1800 rpm coating speed. The figure 5.3(a, b) is showing the seed layer and grown ZnO nanorods at 1800 rpm coating speed of seed solution. The seeds are well distributed on the surface of substrate as shown in figure 5.3(a) which results in the

highly distribution of ZnO nanorods on the substrate surface. Figure 5.3(b) showing that the well oriented grown ZnO nanorods covered the whole surface of substrate.

The substrate coated at 3000 rpm coating speed has a random distribution of seeds on its surface which highly affected the density of growing ZnO nanorods. The grown ZnO nanorods have less density and poor distribution on the surface of substrate. The seeds randomly distributed on the surface of substrate. Figure 5.3(c, d) is showing the poor distribution of seeds and grown ZnO nanorods on the substrate surface respectively.

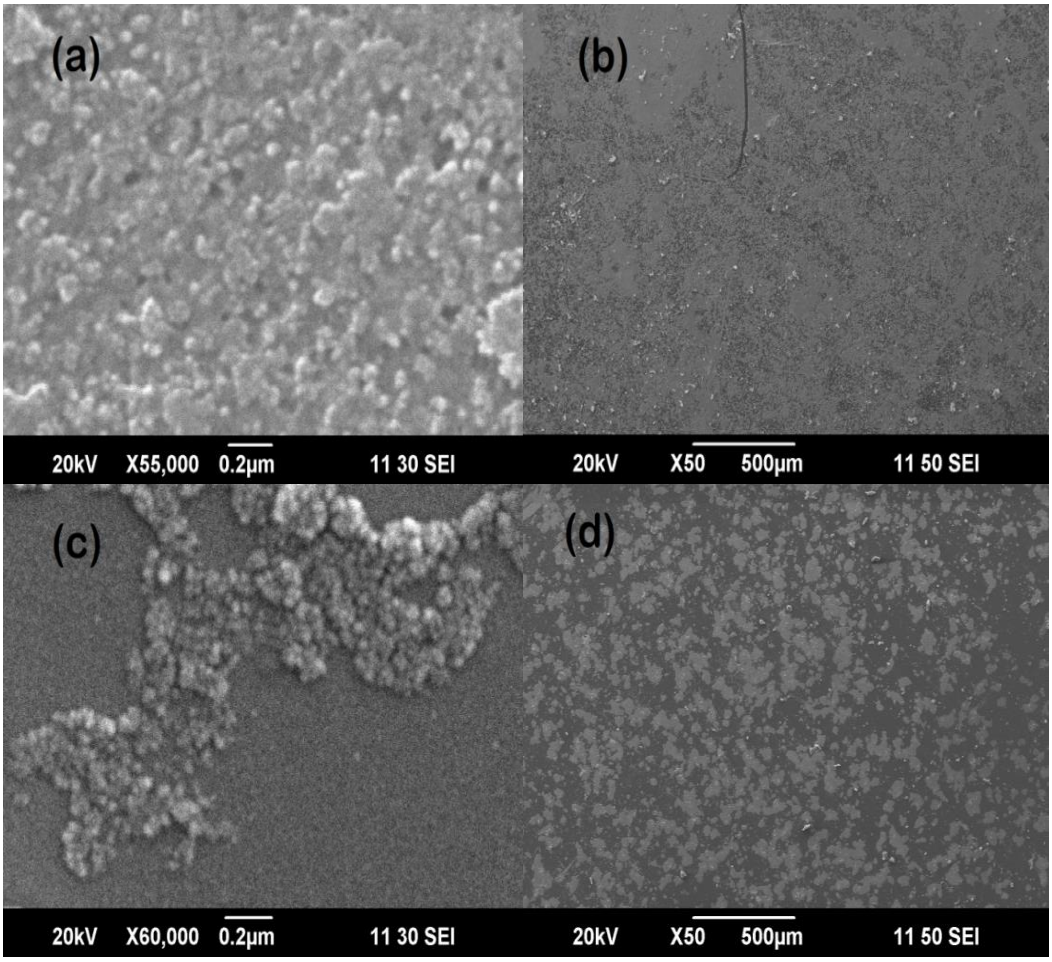

Figure 5.3: Coating speed effect on the distribution of Seeds and ZnO nanorods at 1800 rpm (a, b), 3000 rpm (c, d) respectively.

5.1.2. Effect of different Growth Parameters on ZnO Nanorods

Different growth parameters such as the growth time and growth temperatures were investigated to study their effect on the grown ZnO nanorods. At constant temperatures, growth time was increased from 2-3 hrs which strongly influenced the length and diameter of grown ZnO nanorods.

5.1.2.1. Temperature at 90 °C

In first setup, temperature of the growth solution was kept constant at 90 °C. The growth solution was kept at constant temperature for 2 hrs. It was observed that the length of grown ZnO nanorods were in 100 of nanometers but below the 1 μm and the least observed diameter was about 36 nm. As shown in figure 5.4(a, b), the average diameter and length are about 45 nm and 800 nm respectively.

Secondly, the growth time was increased to 2.5 hrs. The increase in both diameter and length were observed. The least observed diameter was 37 nm and the length was about 1μm. Figure 5.4(c, d) is showing the diameter and length of ZnO nanorods grown at 90 °C for 2.5 hrs. The average diameter was about 48 nm and the average length was about 1 μm.

Further the growth time was increased to 3 hrs. It was observed that the average length of ZnO nanorods was increased from 1 μm to around 1.23 μm. The average diameter of ZnO nanorods was observed around 55 nm. The effects are shown in figure 5.4(e, f).

It is concluded that both the length and diameter was increased by increasing growth time at 90 °C. It was observed that the increasing trend in the length of ZnO nanorods was more than the increasing in diameter. Figures 5.4(a-f) are showing the increasing growth time effect on both diameter and length of ZnO nanorods at 90 °C for 2 hrs, 2.5 hrs and 3 hrs respectively.

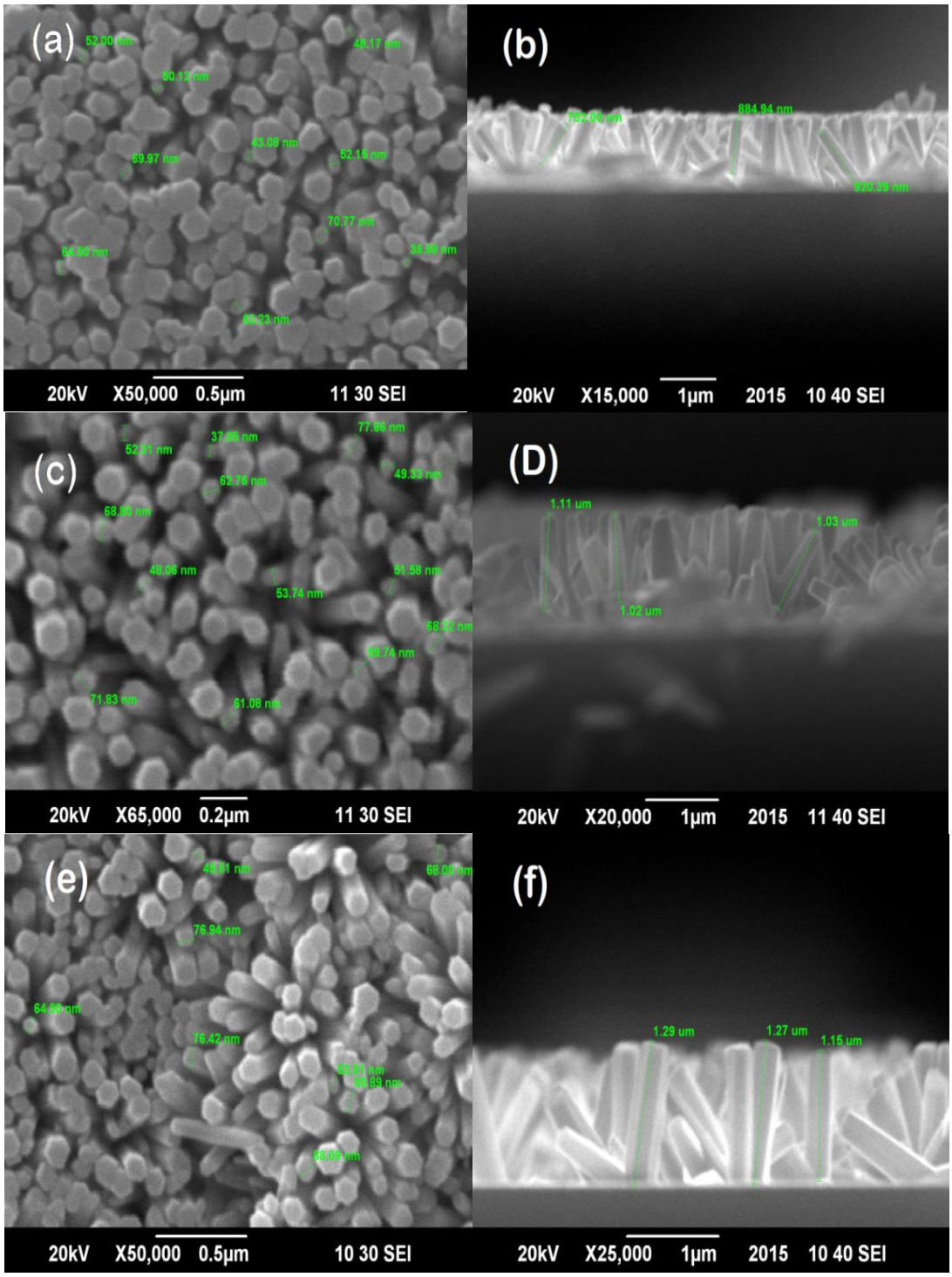

Figure 5.4: Time effect on growth of ZnO nanorods at constant temperature of 90 °C. For 2hrs (a, b), 2.5hrs (c, d) and 3hrs (e, f) respectively.

The graph in figure 5.5 is showing the increasing trend of both diameter and length of nanorods. At constant temperature, both diameter and length of nanorods are increasing with increasing growth time.

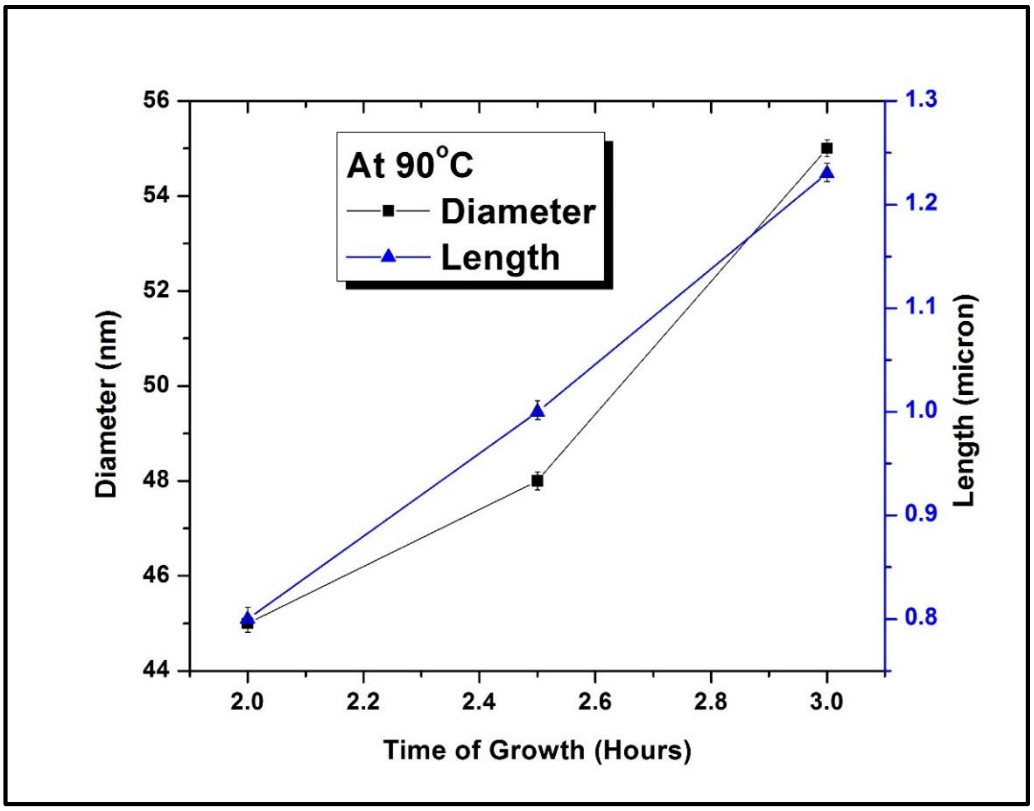

Figure 5.5: Graph showing the relation of diameter and length of ZnO nanorods with increasing growth time at constant temperature 90 °C.

5.1.2.2. Temperature at 95 °C

In next setup, temperature of growth solution was increased to 95 °C while the time intervals were same. In the first time interval, the growth solution was kept in the oven for 2 hrs. It was observed that the average diameter of growing ZnO nanorods was increased from 55 nm to around 65 nm and the length was increased to 1.23 μm. Figure 5.6(a, b) is showing the time and temperature effect on the grown ZnO nanorods.

After observing the effect of 2 hrs, the growth time was increased to 2.5 hrs. As we increased the time of growth solution to 2.5 hrs, it was observed that the length increased to around 1.62 μm to 1.68 μm. The average length was 1.45 μm. The observed average diameter was about 70 nm. Figure 5.6(c, d) is showing the effect of time on as grown ZnO nanorods.

Further the growth time was increased to 3 hrs to study the effect of increased temperature on the grown ZnO nanorods. It was observed that the length of nanorods was increased to about 2 μm. But the diameter was increased above 100

nm. The least diameter was 56 nm and the highest diameter was about 152 nm. So the average diameter of as grown ZnO nanorods was about 90nm. Figure 5.6(e, f) is showing the changed length and diameter of as grown ZnO nanorods.

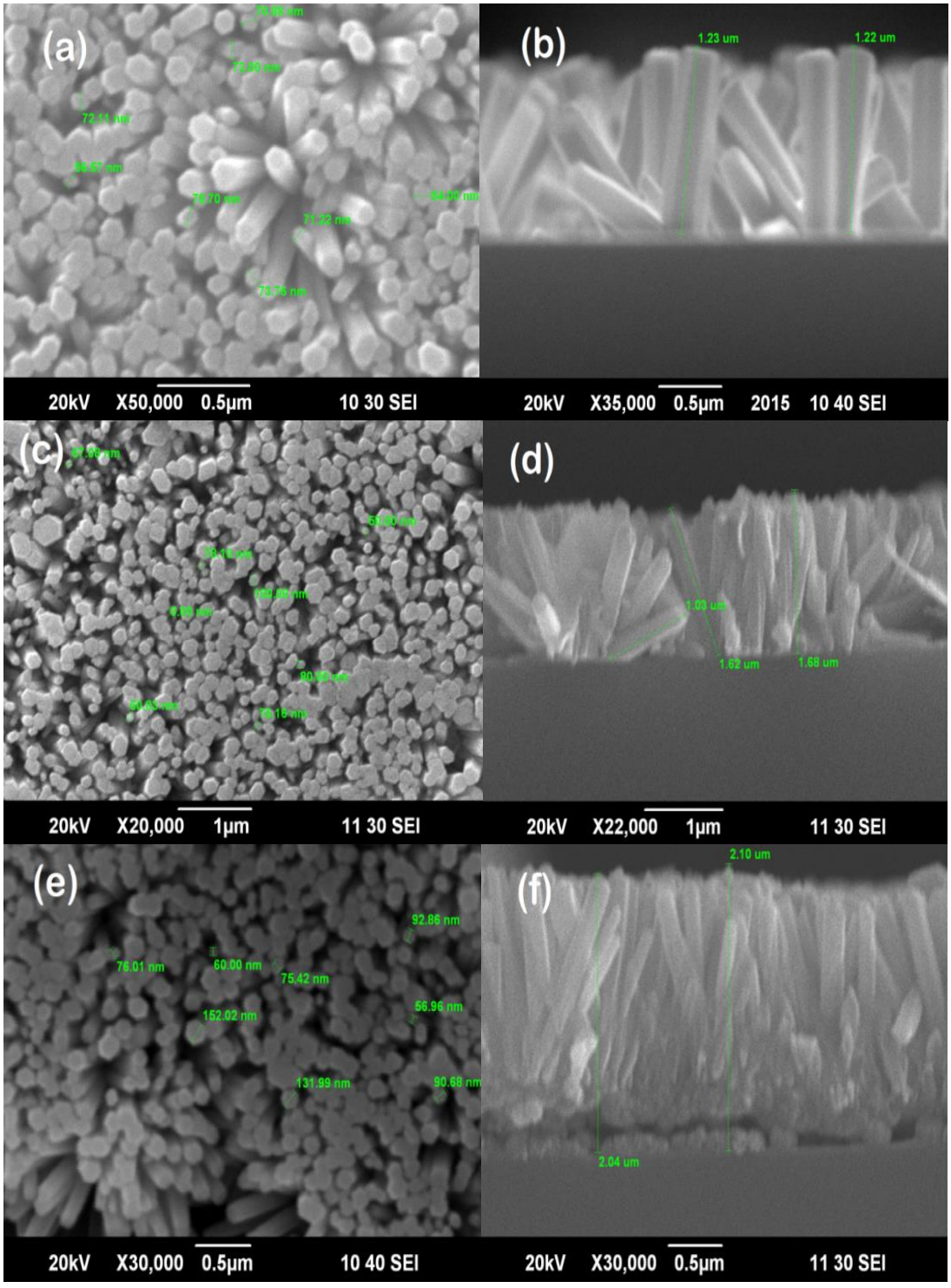

Figure 5.6: The effect of growth time in 2hrs, 2.5, rs, 3hrs at constanrespectivelyre of 95 °C in (a,b), (c, d), (e, f) repectively.

It is observed from above parameters that by changing the time at constant temperature, the increasing growth time also increased the length and diameter of as grown ZnO nanorods. The diameter of as grown ZnO nanorods was increased from 55 nm to around 152 nm and the length was increased from 1.23 nm to 2 μm in the time interval between 2-3 hrs at constant temperature of 95 °C. Figure 5.6(a-f) is showing the whole effect.

The figure 5.7 shows the relation between diameter and length of nanorods with growth time. As growth time increased, both length and diameter of nanorods are also increased at constant temperature of 95 °C.

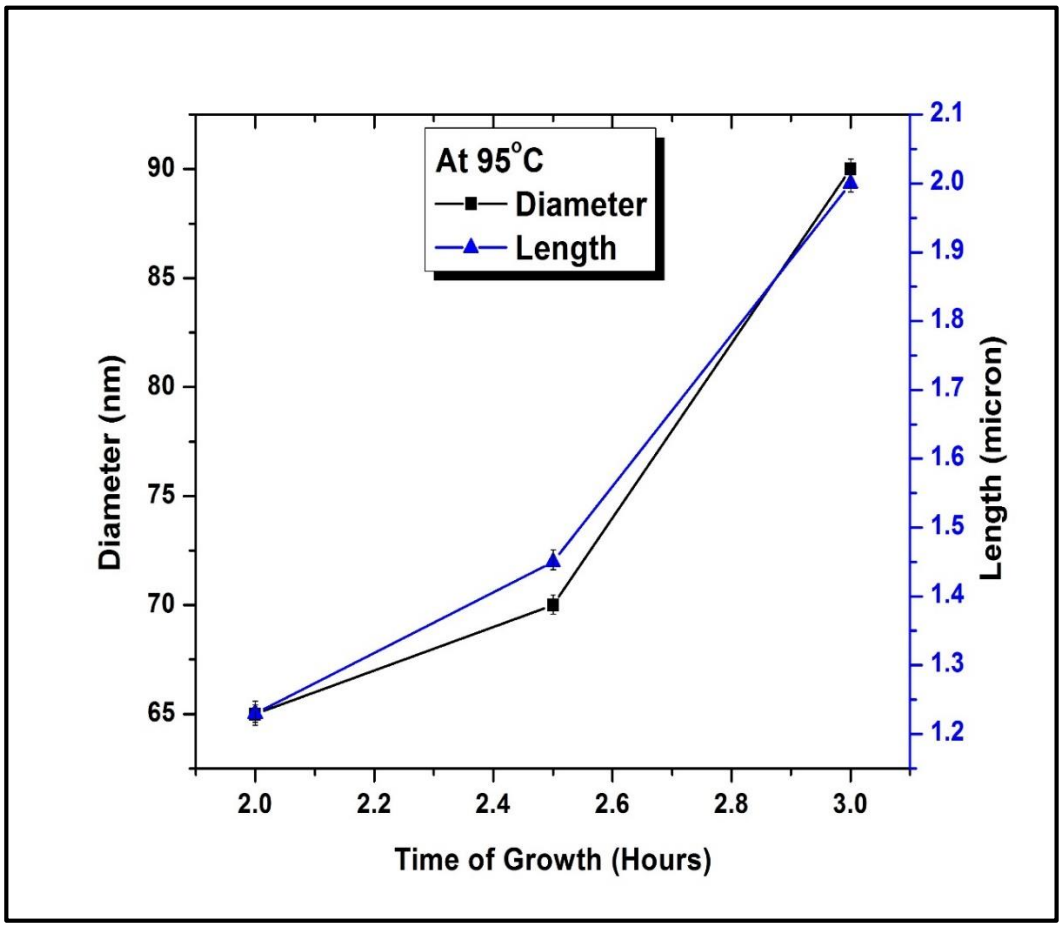

Figure 5.7: Graph showing relation of diameter and length of ZnO nanorods with increasing growth time at constant temperature of 95 °C.

5.1.2.3. Temperature at 100 °C

At the end the growth temperature was increased to 100 °C. In the first time interval, the growth solution was placed in the oven at 100 °C. It was observed that the as grown ZnO nanorods in this time duration have the diameter in the range of 80 nm-154 nm. And the observed length was about1. 60 μm-170 μm. The average

diameter and length were 130 nm and 1.70 μm respectively. So it can be concluded that the temperature increased the both diameter and length of the ZnO nanorods as shown in figure 5.8(a, b).

Further the time interval increased to 2.5 hrs at constant temperature of 100 °C. It was observed that the diameter of ZnO nanorods increased to 200 nm. The least observed diameter was 200 nm and the average diameter was observed around 210 nm.The length was also increased in this time duration. The observed length was 2.20 μm. So it can be seen in figure 5.8(c, d) that the both length and diameter was increased in this time duration.

By increasing growth time to 3 hrs at constant temperature, the length and diameter of nanorods increased slowly. The average diameter were 224 nm and the observed length was increased to around 2.41 μm. Figure 5.8(e, f) shows the both effect in diameter and length of as grown ZnO nanorods.

It can be concluded that both diameter and length of as grown ZnO nanorods were increased in time duration of 2 hr, 2.5 hrs and 3 hrs at 95 °C. But the diameter is increased more than the increase in length. Figures 5.8 (a-f) are showing the effect of all time durations on as grown ZnO nanorods.

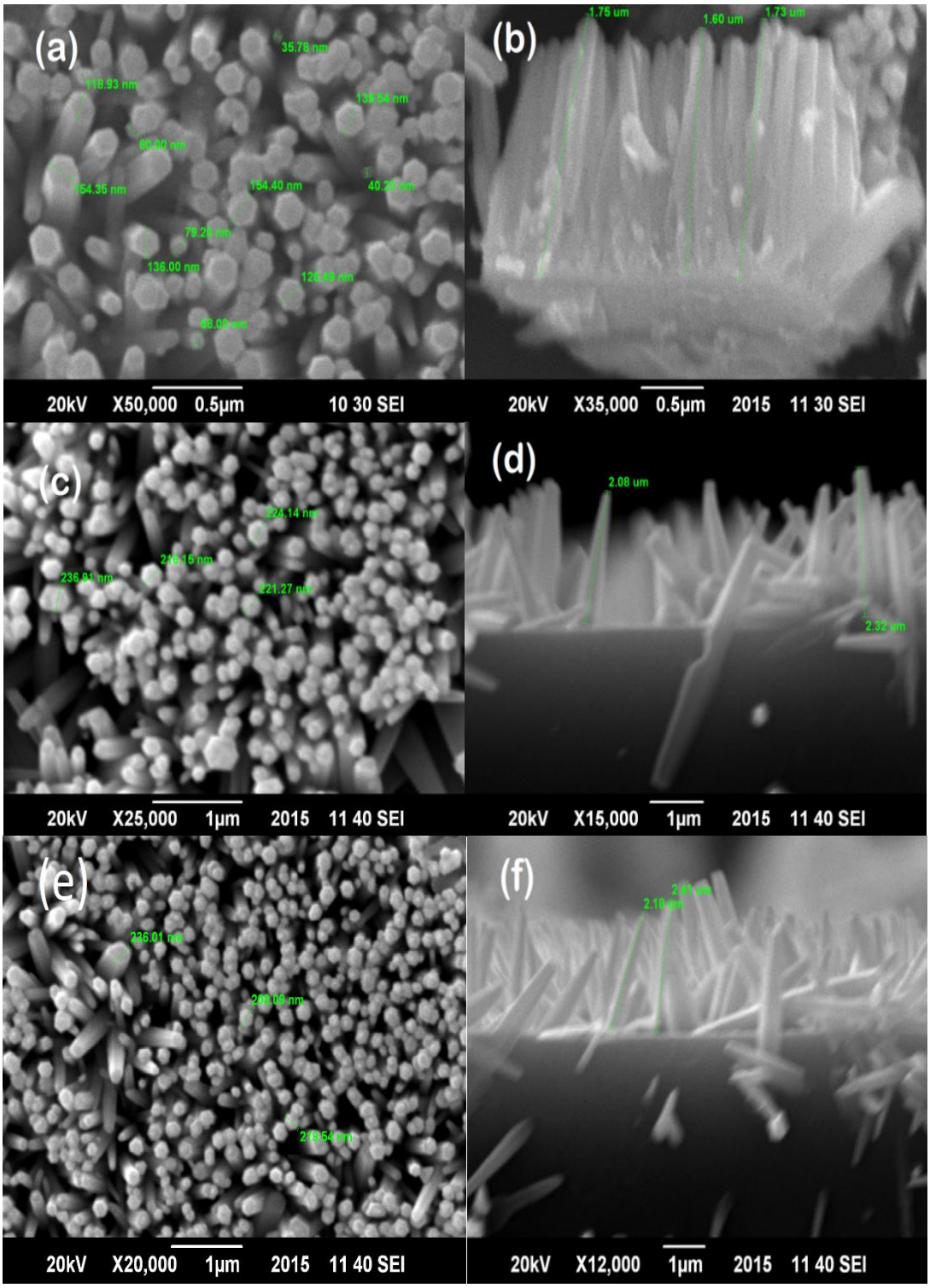

Figure 5.8: 2 hrs, 2.5 hrs and 3 hrs effect on growth of ZnO nanorods at constant temperature of 100 °C respectively.

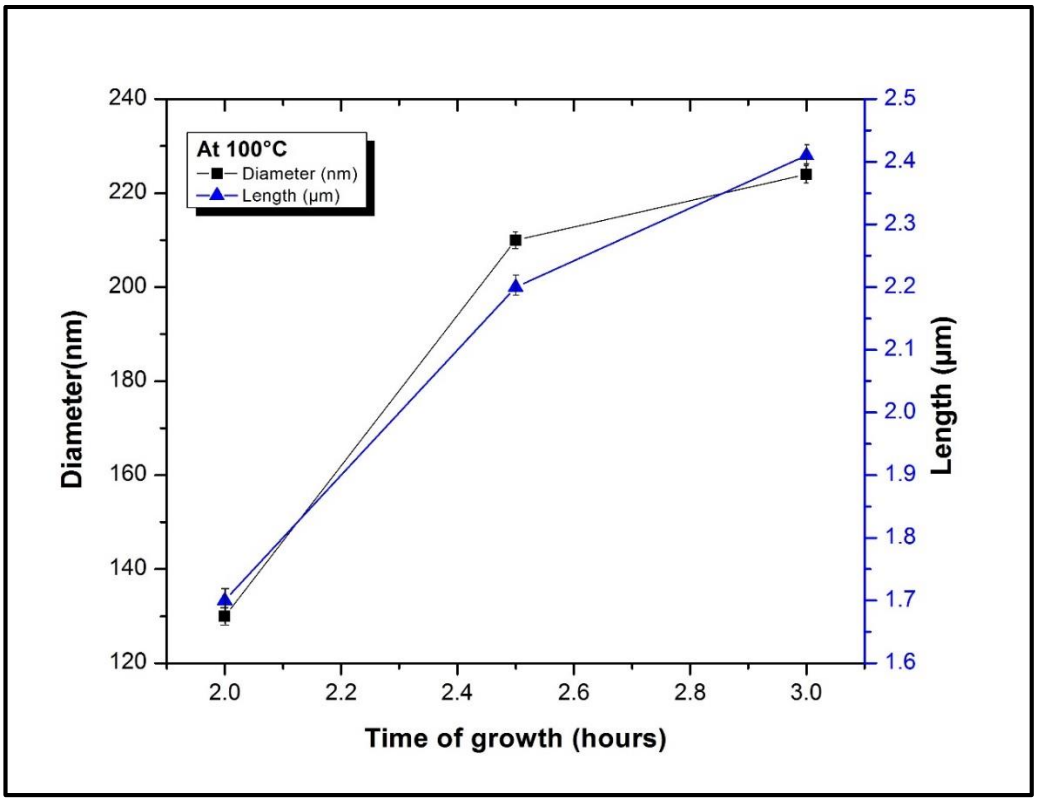

Figure 5.9: Graph showing the effect on diameter and length of ZnO nanorods with increasing growth time at constant temperature of 100 °C.

Figure 5.9 shows the graph between growth time and length and diameter of nanorods. Both diameter and length are increasing with increasing growth time at constant temperature 100 °C.

We used the best optimum conditions for the preparation of sample for the final device fabrication. The substrate coated with 50 μl of seed solution at 1800 rpm. Than annealed the substrate for 30 mins at 250 °C. The substrate was placed in a solution for the growth of nanorods at 95 °C for 2 hrs. Figure 5.10 shows the SEM images of prepared sample.

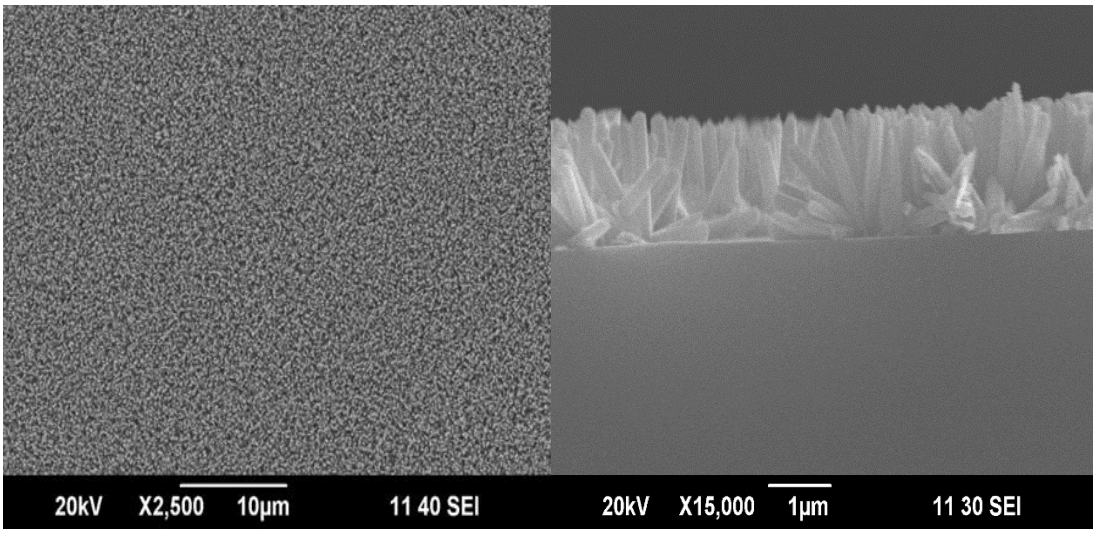

Figure 5.10: SEM images of prepared sample for the final device fabrication.

5.2. Structural Analysis

The X-ray diffraction measurements were collected on STOE powder diffractometer using Cu Kα-radiation (λ= 1.54 Å). The scan range of angle 2θ between 20° to 60°. Xpert High Score software was used to retrieve the XRD data.

Figure 5.11 shows the XRD pattern of ZnO nanorods. The pattern shows the strong intensity peak at 34.422 degrees in (0002) plane. The strongest peak in (0002) plane confirms that the grown nanorods are highly crystalline and preferentially oriented along the c-axis perpendicular the substrate. It evidences the high quality wurtzite hexagonal ZnO structure. The increasing trend in peak of (0002) plane is showing that the orientation of the nanorods increased with increasing growth time and temperature. The lattice parameters were a= 3.249 Å and c=5.206 Å which falls in $P6_3mc$ space group (JCPDS) [63, 64].

Table 5.1: JCPDS XRD data for ZnO.

XRD Peak	2θ (degree) JCPDS	2θ (degree) Observed
(100)	31.770	31.783
(002)	34.422	34.467
(101)	36.253	-
(102)	47.539	-
(110)	56.603	-

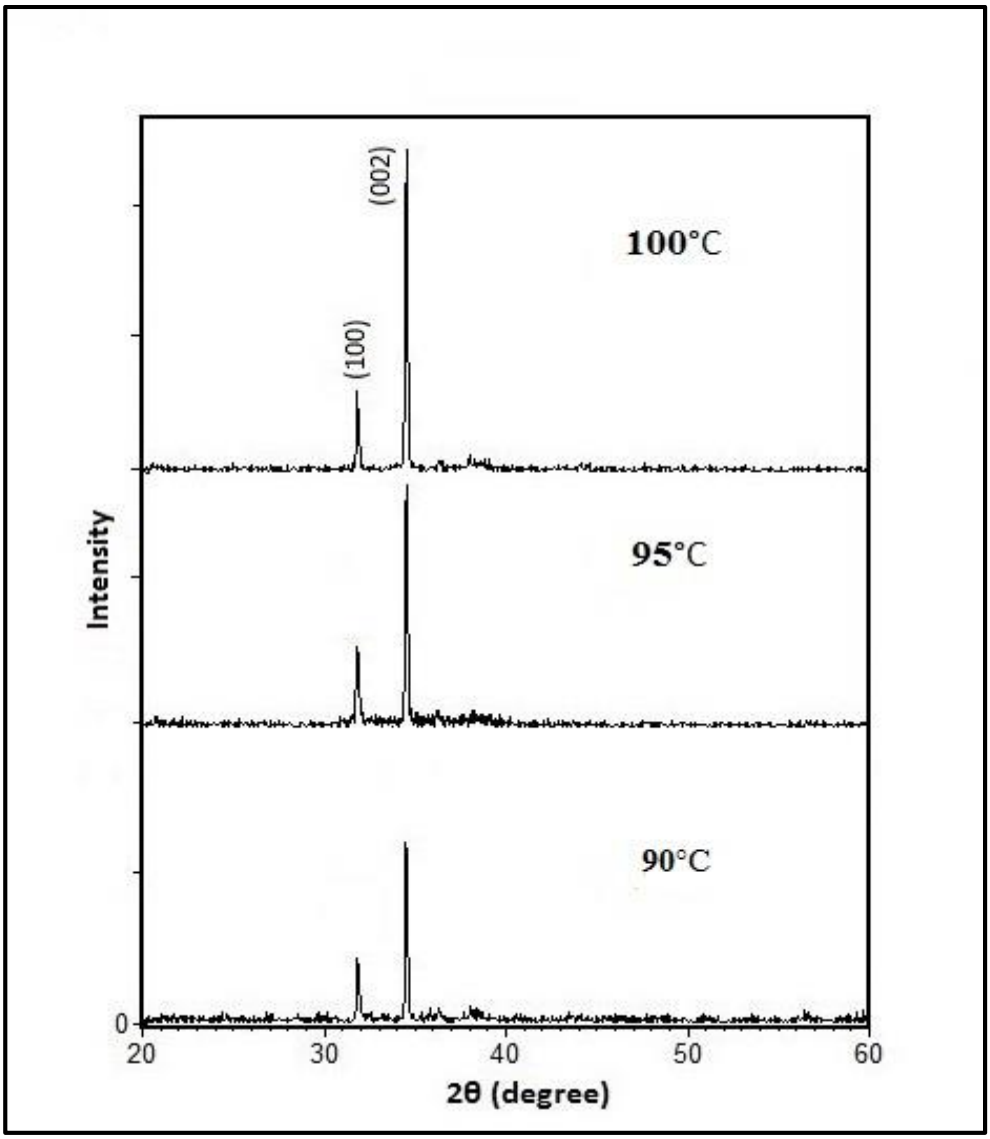

Figure 5.9: XRD pattern of ZnO nanorods for different growth time and temperatures.

Figure 5.12 shows the XRD pattern for the sample we have used for the final device fabrication. The sample has the well oriented ZnO nanorods along the c-axis.

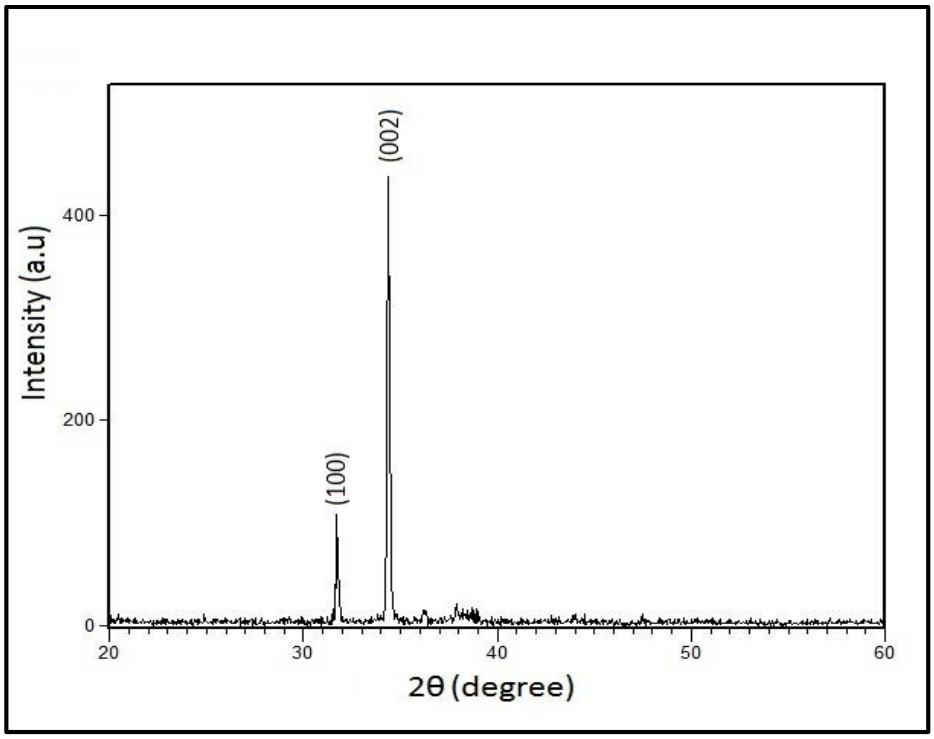

Figure 5.10: XRD patterns of ZnO Nanorods.

5.3. UV-Vis Analysis

To investigate the optical properties of as grown ZnO nanorods, UV-Visible spectroscopy was performed at room temperature. The UV-absorption spectra of as grown ZnO nanorods dispersed in ethanol are shown in figure 5.13. The figure 5.13 shows a prominent, exciton band at 374nm. The absorption edge at 374 nm is blue shifted with respect to bulk absorption edge which has the exciton band at 376 nm. This shift is due to the nano size effect of synthesized ZnO. The lower the diameter of nanorods, the higher the quantum confinement exciton effect is, which coupled the confined electron and holes in a small area and permits them to move in quantum well only. The quantum confinement effect may not be that much stronger here due to the diameter of ZnO nanorods between 30-50 nm. Due to the specific experimental conditions, different energy levels were produced in the ZnO nanorods. So the existence of these higher defect densities at the surface of nanorods is the responsible for this blue shift in UV-absorption spectrum of as grown ZnO nanorods [65].

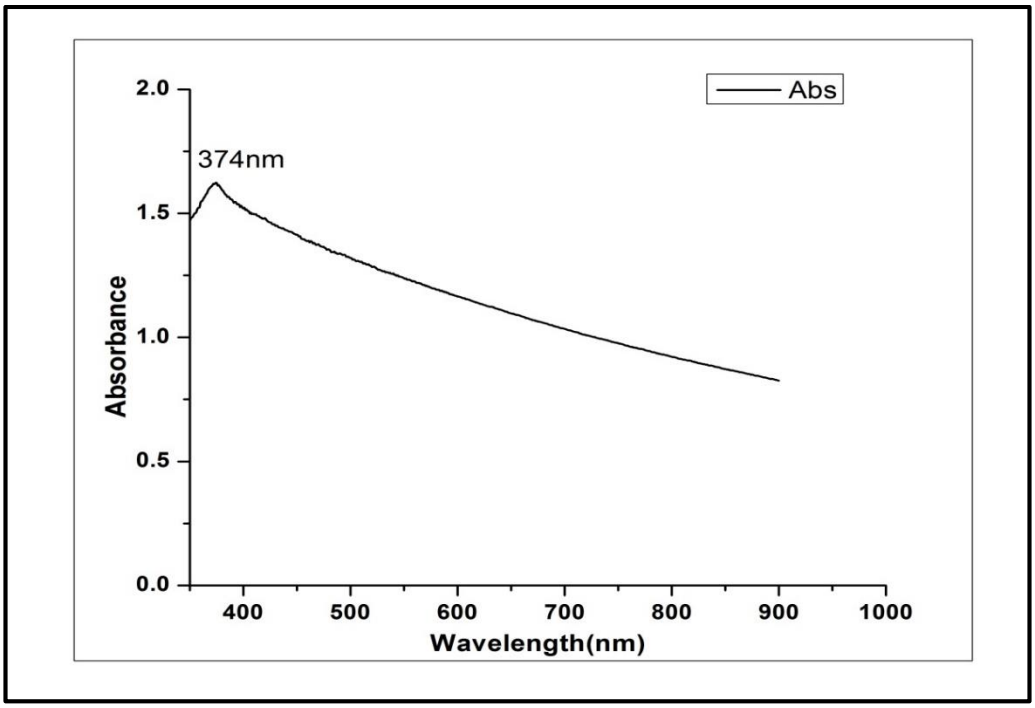

Figure 5.11: UV-absorption Spectra of as grown ZnO Nanorods.

5.4. FTIR Spectroscopy

Fourier transform infrared spectrometer was used to record the Fourier transmission infrared (FT-IR) spectra of the as grown ZnO nanorods powders as pellets in KBr (without moisture). Figure 5.14 shows the room temperature FTIR spectrum of ZnO nanorods in range of 300–4500 cm^{-1}. The obtained FTIR spectrum shows a strong peak at 395 cm^{-1}. This 395 cm^{-1} band corresponds to E_2 mode of wurtzite hexagonal ZnO and can be assigned to the Zn–O stretching vibration modes. The two peaks at 1006 cm^{-1} and 1238 cm^{-1} attributes to the C–O stretching mode absorbed from the atmosphere. The strong peak at 1382 cm^{-1} can be attributed to the symmetric stretching of carboxylate group (COO–), which is most probably from the small leftovers of zinc acetate used in reaction. The peak at 1633 cm^{-1} is associated to the C=O stretching vibration. The broad absorption peak around 3435 cm^{-1} is due to O-H stretching due to the absorption of water molecules at surface of ZnO nanorods in growth reaction [65].

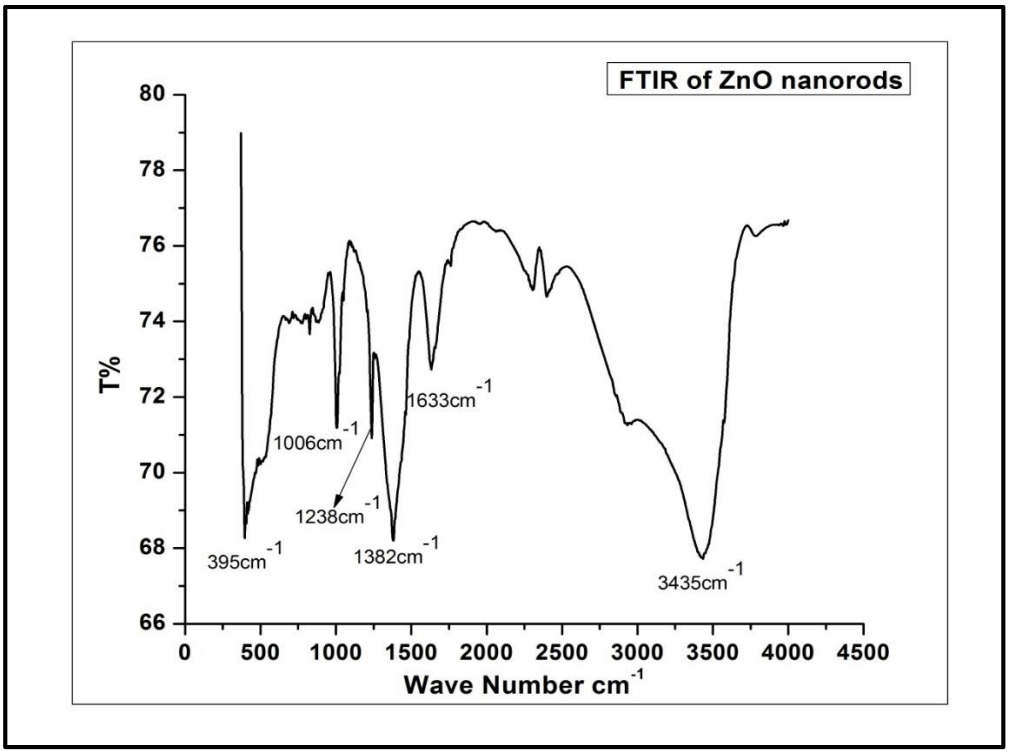

Figure 5.12: FTIR absorption spectrum of ZnO nanorods

5.5. Photoluminescence

The photoluminescence (PL) measurement of the sample was carried out by photoluminescence spectroscopy. The room temperature PL spectrum of growing ZnO nanorods are shown in figure 5.15. It can be observed that there are three peaks in PL spectrum. The recombination of free excitons in PL measurements occurs within the penetration depth from the top of ZnO nanorods. The band edge transition of ZnO can be observed around 381 nm. The Only sharp peak in UV region showed that the as-grown ZnO nanorods have lower density of deep-level defects such as Zn and O vacancies. The deep level emissions are observed for ZnO nanorods centered at 540 nm (green emission) and 680 nm (red emission) [66]. The recombinations of free excitons originate the UV emission. The recombination between the conduction band and zinc interstitial (Zn_i) energy level to oxygen vacancy (V_o) and oxygen interstitial (O_i) cause the green and red emission respectively. Also, the green emission can be attributed to the Zn_i and V_{Zn} defect pairs. So the exact origin of green emission is still an open question and further study is required for its complete identification. The orange emission centered at 650 nm corresponds to the oxygen-rich samples. The band edge emission centered at 381 nm in ZnO nanorods is showing the high crystalline quality of ZnO nanorods [67].

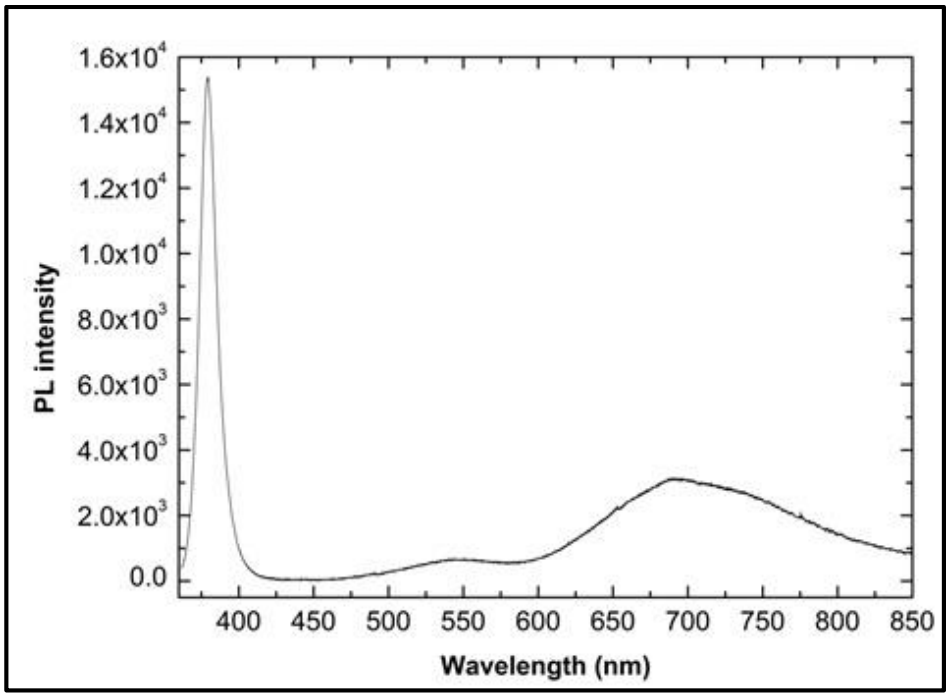

Figure 5.13: Room Temperature PL spectra.

5.6. Electroluminescence

The luminescence properties of the fabricated LED were carried out by electroluminescence measurement. Figure 5.16 shows the room temperature electroluminescence spectrum of the fabricated LED.

A 25 V forward bias current was applied. The recombinations in EL measurements occur at the interface of ZnO and GaN. A broad band emission from the EL spectrum can be observed, which covered the visible spectrum ranges from 440 to 700 nm. A strong blue peak centered at 450 nm can be observed. The blue peak centered at 450 nm is due to the transition from the conduction band of n-ZnO to acceptor levels of p-GaN [66]. Oxygen interstitials (O_i) ranging from 620 nm with bandgap energy 1.99 eV to 690nm with bandgap energy 1.79 eV are the origins for the red emissions in ZnO. The orange-red peaks are due to the band transitions from Zn interstitials (Zn_i) to oxygen interstitials (O_i) defect levels. This emission is approximately centered at 597 nm with a bandgap energy of 2.07 eV [69].

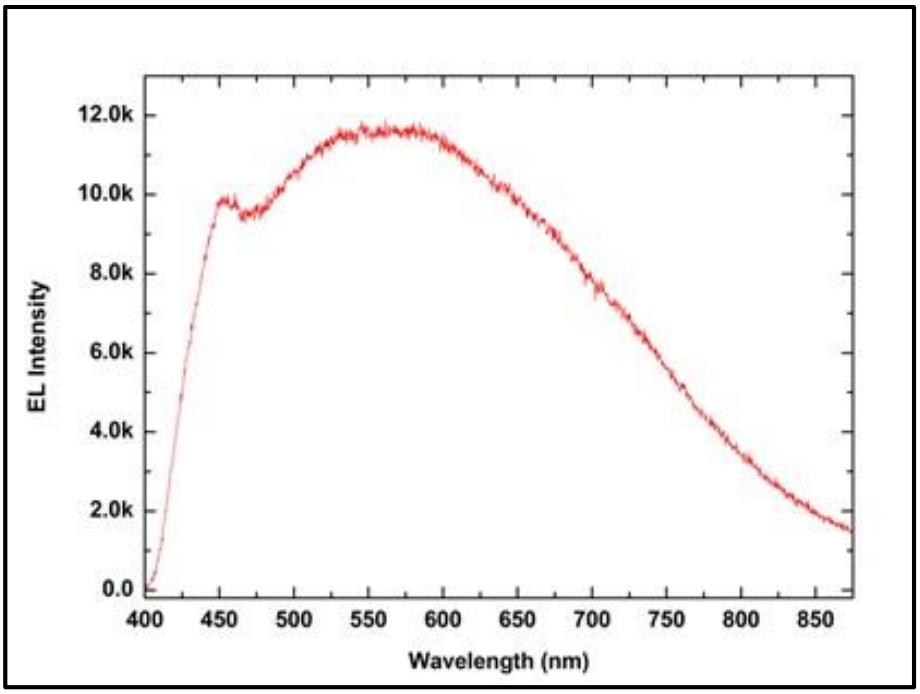

Figure 5.14: The room temperature EL spectrum of n-ZnO/p-GaN heterojunction based LED.

The green emissions centered at 550 nm in EL spectrum. The as-grown ZnO nanorods have the green emissions centered at 2.33 eV. So its energy is close to the oxygen interstitials below the conduction band. Figure 5.17 shows the energy band diagram of DLE emissions in ZnO [68].

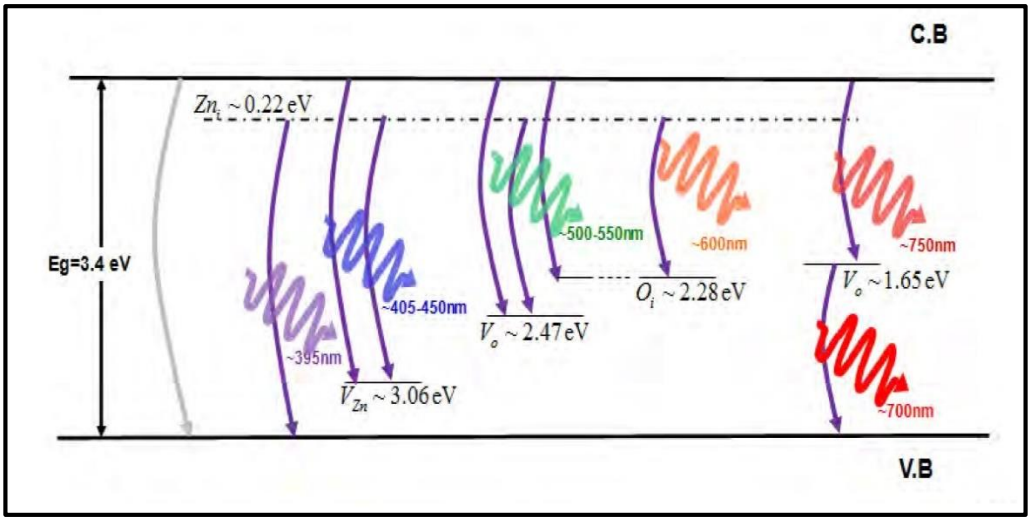

Figure 5.15: ZnO energy bandgap diagram for DLE emissions [68].

Different reasons have been discussed on the origins of n-ZnO/p-GaN heterojunction emissions. Divergence mainly exists in where the emissions from the ZnO side, GaN side [70-72], or from the interface between ZnO and GaN have the

divergence [73]. It was confirmed that the light emission at 450 nm in our EL spectra is mainly originated from the GaN layer. ZnO and GaN have the electron affinities (χ) 4.35 and 4.20 eV respectively, and both have the bandgap with 3.37 and 3.39 eV respectively [74]. The energy band diagram can be drawn according to these values of the bandgap and carrier affinities. The figure 5.18(a) shows the energy band diagram. Both electrons and holes have the equal barrier. Electrons have the barrier of

$$\Delta Ec = \chi\,(ZnO) - \chi\,(GaN) = 0.15\ eV$$

And holes have the barrier of

$$\Delta Ev = Eg(ZnO) + \chi\,(ZnO) - Eg(GaN) + \chi\,(GaN) = 0.12\ eV$$

Since n-ZnO have the both larger values of the carrier concentration and carrier mobility (2.98 x 10^{18} cm^{-3} and 27.1 $cm^2\ V^{-1}\ s^{-1}$) then the values of p-GaN (2.18 x 10^{17} cm^{-3} and 3.14 $cm^2\ V^{-1}\ s^{-1}$), so it is hard to block the electrons in the region of n-ZnO. They will be recombined with holes by injecting them into the p-GaN region as showing in Figure 5.18(b). So by controlling the injection of electrons and holes, EL spectra of the n-ZnO/p-GaN LEDs can be tuned.

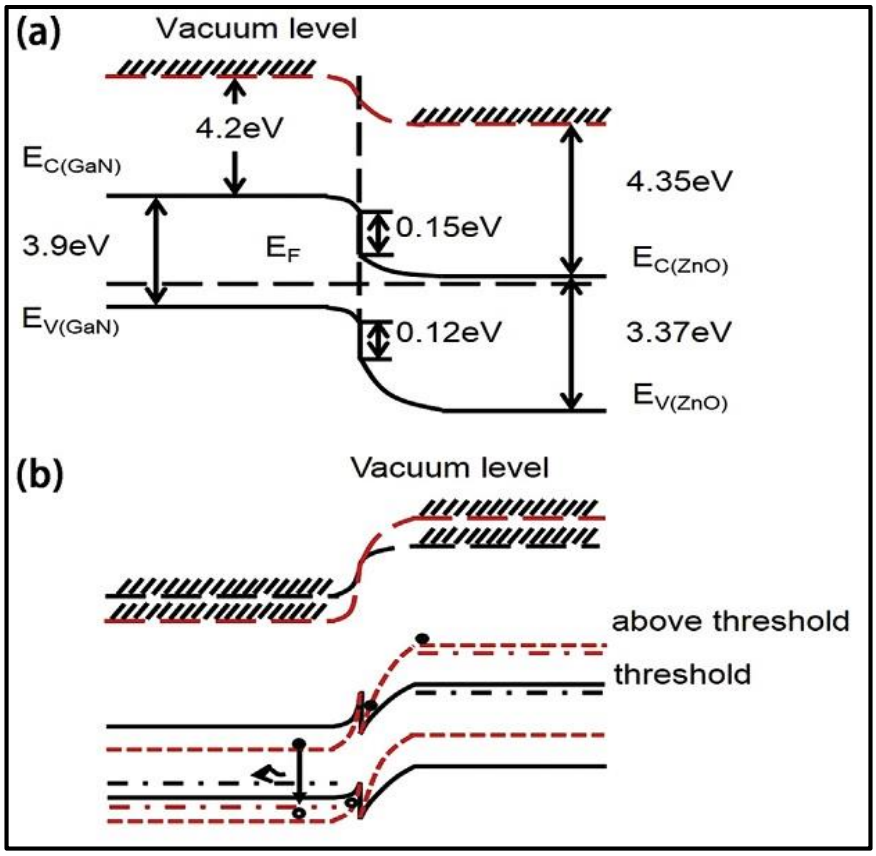

Figure 5.16: (a) Energy band diagram of n-ZnO/p-GaN heterojunction before biased voltage (b) Around and above threshold forward bias.

5.7.Electrical Properties

The typical I-V curves for n-ZnO/p-GaN heterojunction LED is shown in the figure 5.19. The room temperature I-V characteristics measured by the biased voltage varied from -40 V to +40 V. The figure showing the obvious rectifying behavior of the LED with a threshold voltage of 3.8 V. Since the applied voltage was higher than the threshold turn-on voltage, the current started to rise rapidly with the bias voltage. This is the characteristics of a diode [75].

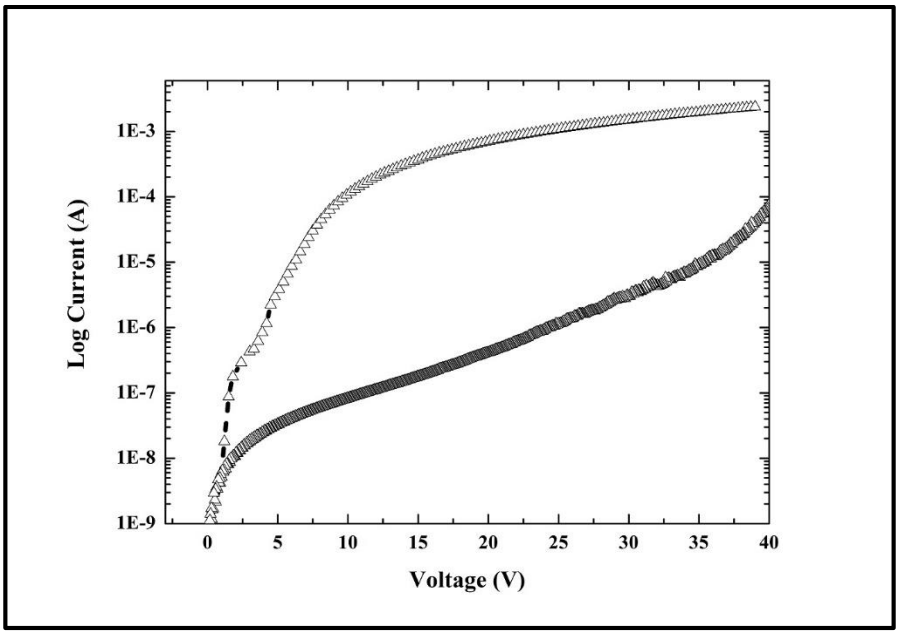

Figure 5.17: Typical IV curve of n-ZnO/p-GaN heterojunction based LEDs with forward bias and reverse bias.

The rapid annealing of the contacts, enhanced the ohmic contacts. The contacts were annealed rapidly for 1 minute at 600 ºC. No current delay at forward bias in curves showed the good ohmic contacts at both interfaces of metal/n-ZnO and metal/p-GaN. But a small breakdown voltage showed the junction leakage current at the interface. In first step, the recombination of carriers started, but no current flow. In second step, the voltage started to flow through the circuit and we have the threshold voltage. At the end, the curve reached to saturation current [76].

Figure 5.20 showed the energy band diagram at (a) normal, (b) forward bias and (c) reverse bias. In normal condition when there is no voltage applied, the depletion region is normal and Fermi level is equal on both sides. When the forward bias voltage is applied, the depletion region of both materials starts to become flat. Fermi level of n-ZnO slightly shifted upward than the p-GaN interface. There is a decrease in the energy barrier for the mobility of carriers. While in reverse bias, the depletion region steep and there is an increase in energy barrier. The current only pass by the tunnelling of mobility carriers through the interface of both materials [77].

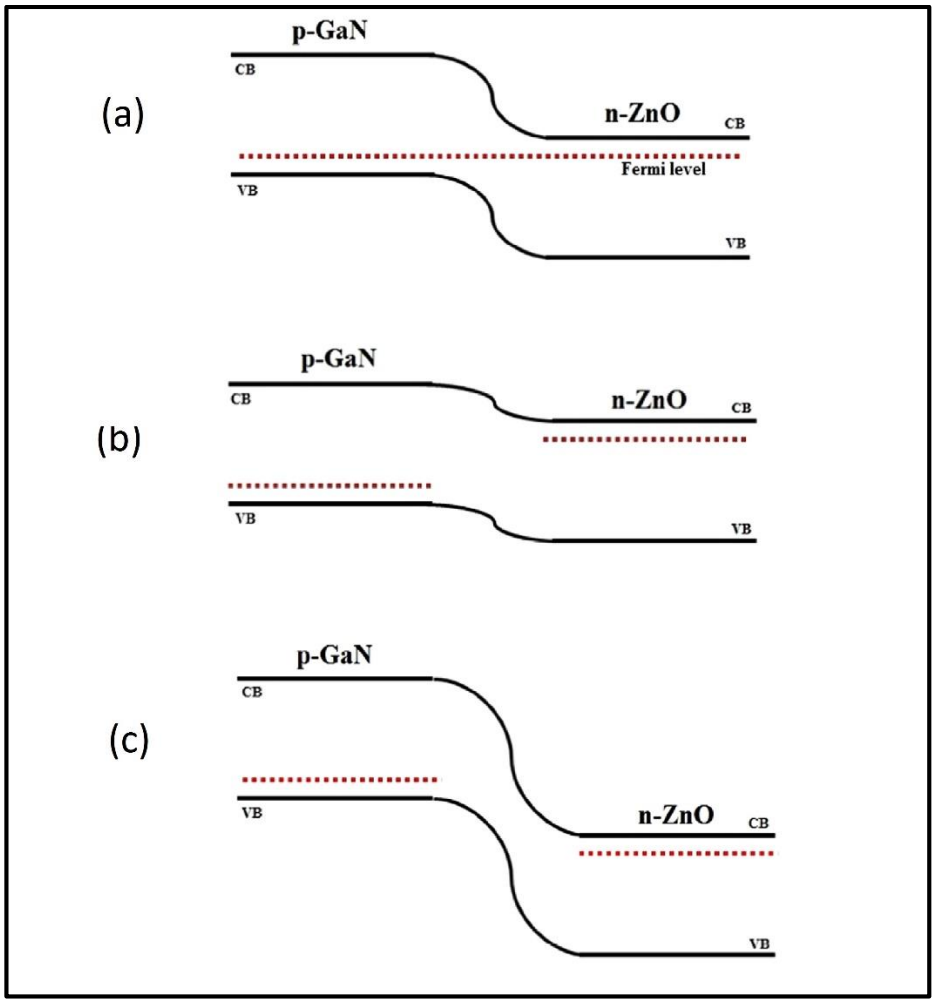

Figure 5.18: Energy band diagram between n-ZnO and p-GaN at (a) normal, (b) forward bias and (c) reverse bias [77].

6. Summary & Future Works

6.1. Conclusion

In this research work, high density one-dimensional ZnO nanorods were grown with controlled diameter. Well aligned ZnO nanorods were grown on GaN substrate. Low temperature and an economical chemical bath deposition method were employed to grow the one-dimensional nanorods. Different parameters were investigated to study their effect on the growth of ZnO nanorods, such as growth temperature, growth time, annealing and effect of seed layer etc. findings of this study are summarized below:

- It was observed that by increasing the concentrations of seed solution on the substrate surface, the density of growing ZnO nanorods also increased. Among the concentrations of 30 µl, 50 µl and 70 µl best uniformity was obtained by the seed layer concentration of 50µl.
- Seed layer coated at 1800 rpm was uniformly dispersed over the whole surface of substrate and resulted in uniform distribution of ZnO nanorods as compared to the substrate coated at the speed of 3000 rpm.
- The growth time and temperature also have the strongest effect on the diameter and length of the as grown ZnO nanorods. The diameter and length of ZnO nanorods were increased from 36 nm-60 nm and 800 nm-1.27 µm respectively, when the growth solution was placed at 90 °C for 2 hrs, 2.5 hrs and 3hrs respectively. At 95 °C, the diameter and length of ZnO nanorods increased from 55 nm-152 nm and 1.23 µm-2 µm when the growth solution time set at 2 hrs, 2.5 hrs and 3 hrs respectively. When the growth solution placed at 100 °C, the diameter and length of ZnO nanorods increased from 80-200 nm and 1.60 µm-2.41 µm in the time of 2hrs and 2.5 hrs respectively. By increasing growth time to 3 hrs, the average diameter were 224 nm and the observed length was increased to around 2.41 µm.
- Intended average diameters (40 nm-60 nm) of the ZnO nanorods were obtained at growth temperature of 90 °C - 95 °C in growth time of 2.5 hrs.

- The UV-Vis spectra of as grown ZnO nanorods show the absorption at 374 nm which conforms closely to the literature value of 376 nm.
- The FTIR spectra showed the absorption peak at 395cm^{-1} which is attributed to the Zn-O stretching vibration mode.
- The XRD pattern showed highest peak at angle 34.467 degrees of (0002) plane. This confirmed that the ZnO nanorods were well aligned along the c-axis.
- The Photoluminescence showed emission of the green and orange-red deep level. The sharp UV emission at 381 nm shows that the nanorods have lower density of deep level defects and high degree of crystallinity. The green and red emissions were observed at 540 nm and 680 nm due to the surface defects.
- The electroluminescence spectrum of fabricated LED showed the broad emission peak ranging from 440 nm to 700 nm. The transition from the conduction band to the acceptor level of GaN at 450 causes the blue emission. Red emissions have ranged from 620-690 due to the Zn interstitials. Orange-Red emissions at 597nm is due to the transition from Zn interstitials to Oxygen interstitials. Green emissions centered at 550 nm are supposed to be oxygen interstitials below the conduction band. So the fabricated LED almost covered the whole visible emissions.
- The current voltage characteristics also known as IV curves showed the turn on voltage at 3.8. Rapidly annealed contacts showed no current delay in forward bias.

6.2. Future Work Suggestions

In this research work, different key points on the growth of ZnO nanorods have been identified, however, more studies are required to obtain the complete description of nanorod's growth. More parameters can also vary to obtain the best results for the proposed applications.

ZnO nanotubes can also synthesis by introducing some precursors in the growth method or by changing some parameters. ZnO nanorods/nanotubes can be grown on flexible substrate for the flexible electronics by using this simple and economical chemical method.

Different one-dimensional nanostructures such as nanowires, nanobelts etc. can be grown by using this simple method according to their applications.

The as grown ZnO nanorods can also be altered according to different applications like biosensors, solar cells, electronic devices etc.

Different 1D nanostructures of different materials can also be grown by using this economical method with easy techniques to alter the growth parameters according to their use in different applications.

References

[1] A. Janotti and C. G. Van de Walle, Rep. Prog. Phys. **72**, 126501 (2009)

[2] M. Willander et al., Nanotechnology, **20**, 332001 (2009)

[3] Z. L. Wang, Materials Today **7**, 26 (2004)

[4] U. Ozgur et al., J. Appl. Phys. **98**, 1 (2005)

[5] Peter Klason, Zinc oxide bulk and nanorods, A study of optical and mechanical properties, PhD thesis, University of Gothenburg, (2008)

[6] S. B. Ogale, Thin films and Heterostructures for Oxide Elelectronics (New York: Springer) (2005)

[7] C. Jagadish and S. J. Pearton (ed) Zinic Oxide Bulk, Thin Films, and Nanostructures (New York: Elsevier) (2006)

[8] C. X. Wang, G. W. Yang, H. W. Y. H. Han. J. F. Luo, C. X. Gao, and G. T. Zou, Appl. Phys. Lett. **84**, 2427 (2004)

[9] X. D. Chen, C.C. Ling, S. Fung, C. D. Beling, Y. F. Mei, R. K. Y. Fu, G. G. Siu, and P. K. Chu, Appl. Phys. Lett. **88**, 132104 (2006)

[10] Y. Alivov, J. E. V. Nostrand, D. C. Look, B. M. Ataev, and A. K. Omaev, Appl. Phys. Lett. **83**, 2943 (2003)

[11] R. W. Chuang, R. X. Wu, L. W. Lai, and C. T. Lee, Appl. Phys. Lett. **91**, 231113 (2007)

[12] M. K. Wu, Y. T. Shih, W. C. Li, H. C. Chen, M. J. Chen, H. Kuan, J. R. Yang, and M. Shiojiri, IEEE Photon. Technol. Lett. **20**, 1772 (2008)

[13] S. J. An, and G. C. Yi, Appl. Phys. Lett. **91**, 123109 (2007)

[14] A. M. C. Ng, Y. Y. Xi, Y. F. Hsu, A. B. Djurisic, W. K. Chan, S. G. wo, H. L. Tam, K. W. Cheah, P. W. K. Fong, H. F. Lui, and C. Surya, Nanotechnology **20,** 445201 (2009)

[15] http://www1.eere.energy.gov/buildings/ssl/news_detail.html?news_id=15806

[16] N. H. Alvi, S. M. Usman Ali, S. Hussain, O. Nur, and M. Willander, Scripta Materialia 2011, 64, 697.

[17] A. Wadesa, O. Nur, and M. Willander, Nanotechnology 2009, 20, 065710. [3] S. M. Usman Ali, O. Nur, M. Willander, B. Danielsson, Sens. Actuators B 2010, 145, 874.

[18] Y. Li, F. D. Valle, M. Simonnet, I. Yamada and Delaunay, Nanotechnology 2009, 20, 045501.

[19] Z. L. Wang, and J. Song, Science 2006, 312, 242.

[20] C. Jagadish and S. J. Pearton, Zinc Oxide Bulk, Thin Films and Nanostructures, Elseviser Ltd., (2006).

[21] A. Fulati, S. M. Usman Ali, M. Riaz, G. Amin, O. Nur and M. Willander, Sensors 2009, 9, 8911.

[22] B. Meyer, and D. Marx, Phys. Rev. B 2003, 67, 035403.

[23] A. Wander, F. Schedin, P. Steadman, A. Norris, R. McGrath, T. S.Turner, G. Thornton, and N. M. Harrison, Phys. Rev. Lett. 2001, 86, 3811.

[24] V. Staemmler, K. Fink, B. Meyer, D. Marx, M. Kunat, S. G. Girol,U. Burghaus, and Ch. Wöll, Phys. Rev. Lett. 2003, 90, 106102.

[25] C. H. Bates, W. B. White, R. Roy, Science 1962, 137, 993.

[26] C. Jagadish, and S. J. Pearton (eds.), Zinc Oxide Bulk, Thin Films, and Nanostructures (Elsevier, Amsterdam, 2006), p. 1.

[27] C. Jagadish, and S. J. Pearton (eds.), Zinc Oxide Bulk, Thin Films, and Nanostructures (Elsevier, Amsterdam, 2006), p. 1.
[28] D. I. Florescu, L. G. Mourokh, F. H. Pollak, D. C. Look, G. Cantwell, and X.Li, J. Appl. Phys. 2002, 91, 890.
[29] D. Florescu, L. G. Mourok, F. H. Pollack, D. C. Look, G. Cantwell, and X. Li, J. Appl. Phys. 2002, 91, 8902.
[30] A. B. Djurisic and Y. H. Leung, Small 2006, 2, 944.
[31] X. Liu, X. Wu, H. Cao, and R. P. H. Chang, J. Appl. Phys. 2004, 95, 3141.
[32] A. Janotti, and C. G. Van de Walle, Phys. Rew. B 2007, 76, 165202.
[33] Z. Fan, P. Chang, E. C. Walter, C. Lin, H. P. Lee, R. M. Penner, and J. G. Lu, Appl.Phys. Lett. 2004, 85, 6128.
[34] P. Klason, T. M. Borseth, Q. X. Zhao, B. G. Svensson, A. Y. Kuznetsov, and M. Willander, Sol. Stat. Commun. 2008, 145, 321.
[35] S. M. Usman Ali, N.H. Alvi, Z. Ibupoto, O. Nur, M. Willander, B. Danielsson, Sens. & Actuators :B 2011, 2, 241.
[36] M. H. Asif, S.M. Usman Ali, O. Nur, M. Willander, C. Brännmark, P. Strålfors , U. Englund, F. Elinder and B. Danielsson, Biosens. Bioelectron.2010, 25, 2205.
[37] T. J. Hsueh, S. J. Chang, C. L. Hsu, Y. R. Lin, and I. C. Chen, J. Electrochem. Soc. 155, K 152 (2008)
[38] J. X. Wang, X. W. Sun, H. Huang, Y. C. Lee, O. K. Tan, M. B. Yu, G. Q. Lo, and D. L. A. Kwong, Appl. Phys. A 88, 611 (2007)
[39] L. Mai, D. H. Kim, M. Yim, and G. Yoon, Microwave and Optical Technology Letters 42, 505 (2004)
[40] T. P. Yang, H. C. Zhu, J. M. Bian, J. C. Sun, X. Dong, B. L. Zhang, H. W. Liang, X. P.Li, Y. G. Cui, and G. T. Du, Material Research Bulletin 43, 3614 (2008)
[41] K. Liu, M. Sakurai, and M. Aono, Sensors 10, 8604 (2010)
[42] E. Mollow, Proceedings of the Photoconductivity Conference, Breckenridge, R. G, Ed.Wiley, New York, NY, USA, pp-509 (1954)
[43] H. Fabricius, T. Skettrup, and P. Bisgaard, Appl. Opt. 25, 2764 (1986)
[44] K. ul Hasan, N. H. Alvi, J. Lu, O. Nur and M. Willander, Nanoscale Research Letters 6,348 (2011)
[45] M. Nakano, T Makino. A. Tsukazaki, K. Ueno, A. Ohtomo, T. Fukumura, H. Yuji, S. Akasaka, K. Tamura, K. Nakahara, T. Tanabe, A. Kamisawa, and M. Kawasaki, Appl. Phys. Lett. 93, 123309 (2008)
[46] Ya. I. Alivov, E. V. Kalinina, A. E. Cherenkov, D. C. Look, B. M. Ataev, A. K. Omaev,M. V. Chukichev, and D. M. Bagnall, Appl. Phys. Lett. 83, 4719 (2003)
[47] J. B. You, X. W. Zhang, S. G. Zhang, J. X. Wang, Z. G. Yin, H. R. Tan,W. J. Zhang, P.K. Chu, B. Cui, A. M. Wowchak, A. M. Dabiran, and P. P. Chow, Appl. Phys. Lett. 96,201102 (2010)
[48] Z. W. Pan, Z. R. Dai, and Z. L. Wang, Science. **291**, 1947 (2001)
[49] Y. Huang, Y. Zhang, X. Bai, J. He, J. Liu, and X. Zhang, J. Nanosci. Nanotech. **6**, 2566 (2006)
[50] W. L. Hughes, and Z. L. Wang. Appl. Phys. Lett. **86**, 04310 (2005)
[51] S. Baruah, C. Thanachayanont, and Dutta, J. Sci. Technol. Adv. Mater. **9**, 025009 (2008)
[52] T. H. Fang, and S. H. Kang, J. Phys. D: Appl. Phys. **41**, 245303 (2008)
[53] S. J. Young, L. W. Ji, S. J. Chang, T. H. Fang, T. J. Hsueh, T. H. Meen, and I. C. Chen, Nanotechnology **18**, 225603 (2007)

[54] M. Wang, C. H. Ye, Y. Zhang, G. M. Hua, H. X. Wang, and M. G. Kong, J. Cryst. Growth **291**, 33 (2006)
[55] E. L. Greene, M. Law, H. T. Dawud, M. Montano, J. Goldberger, G. Somorjai, and P. Yang, Nano Lett. **5**, 123 (2005)
[56] M. E. Lin et al., Appl. Phys. Lett. **64**, 1003 (1994) 60
[57] H. K. Kim, K. K. Kim, S. J. Park, T. Y. Seong, and I. Adesida, J. Appl. Phys. **94**, 4225 (2003)
[58] G. Binnig, C. F. Quate, and C. Gerber, "Atomic force microscope," *Physical Review Letters* **56**, (1986).
[59] A. R. Clarke and C. N. Eberhardt, *Microscopy techniques for materials science,* Woodhead Publishing, (2002).
[60] R. B. Von Dreele and B. H. Toby, "X-Ray Powder Diffraction," in *Characterization of Materials*, ed: John Wiley & Sons, Inc., 2002
[61] G. D. Gilliland, Mater. Sci. Eng. R**18**, 99 (1997)
[62] N. H. Alvi, S. M. Usman Ali, S. Hussain, O. Nur, and M. Willander, Scripta Materiala 64, 697 (2011)
[63] Z. H. I. Kimleang Khun , Mohamad S. AlSalhi, Muhammad Atif , and A. A. A. a. M. Willander, *materials*, vol. 6, pp. 4361-4374, 2013.
[64] S. K. P. P. K. Samanta, A. Ghosh and P. Roy Chaudhuri, *International Journal of NanoScience and Nanotechnology,* vol. 1, pp. 81-90, 2009.
[65] M. P. D. B.H. Soni, S.V. Bhatt, N. Garg, S.H. Chaki, *JOURNAL OF NANO- AND ELECTRONIC PHYSICS*, vol. 6, p. 04077, 2013.
[66] N. H. Alvi, M. Riaz, G. Tzamalis, O. Nur, and M. Willander, Semiconductor Science and Technology **25**, 065004 (2010)
[67] C. Bekeny, M. Kreye, and A. Waag, J. Appl. Phys. 100, 104317 (2006)
[68] N. H. Alvi, K. ul Hasan, O. Nur, and M. Willander, Nanoscale Research Letters. 6, 130 (2011)
[69] C. H. Ahn, Y. Y. Kim, D. C. Kim, S. K. Mohanta, and H. K. Cho, J. Appl. Phys. 105, 089902 (2009)
[70] Y.I. Alivov, J. Van Nostrand, D. Look, M. Chukichev, B. Ataev, Appl. Phys. Lett. 83 (2003) 2943e2945.
[71] D. Rogers, F.H. Teherani, A. Yasan, K. Minder, P. Kung, M. Razeghi, Appl. Phys. Lett. 88 (2006) 141918.
[72] S. Chang, R.W. Chuang, S.J. Chang, Y. Chiou, C. Lu, Thin Solid Films 517 (2009) 5054e5056.
[73] Q. Yang, W. Wang, S. Xu, Z.L. Wang, Nano Lett. 11 (2011) 4012e4017.
[74] M.C. Jeong, B.Y. Oh, M.H. Ham, J.M. Myoung, Appl. Phys. Lett. 88 (2006) 202105.
[75] Shrawan Jha, J.-C. Q., Oleksandr Kutsay, Jaroslav Kovac Jr, Chun-Yan Luan, Juan Antonio Zapien, Wenjun Zhang, Shuit-Tong Lee and Igor Bello. Nanotechnology, 22, 245202 (2011). doi: 10.1088/0957-4484/22/24/24520
[76] Sun-Hong Park, S.-H. K., Sang-Wook Han. Nanotechnology, 18 (2007). doi: 10.1088/0957-4484/18/5/055608
[77] Ahmad Echresh, C. O. C., Morteza Zargar Shoushtari, Omer Nur, Magnus Willander. Journal of Luminescence, 160, 305-310 (2015)